MICROCOPY RESOLUTION TEST CHART

NATIONAL BUREAU OF STANDARDS-1963-A

AFOSR-TR- 83 - 0 8 6 9

(10)

AD-A133 769

Flow Research Report No. 262

Experimental Studies of Unsteady
Phenomena in Boundary Layers

(Annual Technical Report)

By

Mohamed Gad-el-Hak

May 1983

Flow Research Company
A Division of Flow Industries, Inc.
21414-68th Avenue South
Kent, Washington 98032
(206) 872-8500

DTIC
S ELECTF
OCT 20 1983
D

83 10 19 006

Qualified requestors may obtain additional copies
from the Defense Technical Information Service.

Conditions of Reproduction

Reproduction, translation, publication, use and disposal
in whole or in part by or for the United States Government is permitted.

REPORT DOCUMENTATION PAGE		READ INSTRUCTIONS BEFORE COMPLETING FORM
1. REPORT NUMBER AFOSR-TR- 83-0869	**2. GOVT ACCESSION NO.** AD·A133769	**3. RECIPIENT'S CATALOG NUMBER**
4. TITLE (and Subtitle) "Experimental Studies of Unsteady Phenomena in Boundary Layers"		**5. TYPE OF REPORT & PERIOD COVERED** Annual Technical Report 1 May 1982 – 30 April 1983
		6. PERFORMING ORG. REPORT NUMBER FRC-Report No. 262
7. AUTHOR(s) Mohamed Gad-el-Hak		**8. CONTRACT OR GRANT NUMBER(s)** F49620-82-C-0020
9. PERFORMING ORGANIZATION NAME AND ADDRESS Flow Research Company/Flow Industries, Inc. 21414 – 68th Avenue South Kent, WA 98032		**10. PROGRAM ELEMENT, PROJECT, TASK AREA & WORK UNIT NUMBERS** 61102 F 2307/K1
11. CONTROLLING OFFICE NAME AND ADDRESS Air Force Office of Scientific Research/NA Bolling Air Force Base, Washington, DC 20332		**12. REPORT DATE** 5 May 1983
		13. NUMBER OF PAGES 59
14. MONITORING AGENCY NAME & ADDRESS(If different from Controlling Office)		**15. SECURITY CLASS. (of this report)** Unclassified
		15a. DECLASSIFICATION DOWNGRADING SCHEDULE

16. DISTRIBUTION STATEMENT (of this Report)

Approved for public release;
distribution unlimited.

17. DISTRIBUTION STATEMENT (of the abstract entered in Block 20, If different from Report)

18. SUPPLEMENTARY NOTES

19. KEY WORDS (Continue on reverse side if necessary and identify by block number)

Decelerating Boundary Layers; Transition; Unsteady Flows; Flow Visualization Numerical Solution of Orr-Sommerfeld Equation.

20. ABSTRACT (Continue on reverse side if necessary and identify by block number)

The stability of decelerating boundary layer flow is investigated experimentally and numerically. Experimentally, a flat plate having a Blasius boundary layer is decelerated in an 18-m towing tank. The boundary layer becomes unstable to two-dimensional waves which break down into three-dimensional patterns, hairpin vortices, and finally turbulent bursts when the vortices lift off the wall. The unsteady boundary layer equations are solved numerically to generate instantaneous velocity profiles for a range

DD FORM 1473 **1 JAN 73** EDITION OF 1 NOV 65 IS OBSOLETE

20. ABSTRACT

of boundary and initial conditions. A quasi-steady approximation is invoked and the stability of local velocity profiles are determined by solving the Orr-Sommerfeld equation using Chebyshev matrix methods. Comparisons are made between the numerical predicitions and the experimentally observed instabilities.

Flow Research Report No. 262

Experimental Studies of Unsteady Phenomena in Boundary Layers

(Annual Technical Report)

By

Mohamed Gad-el-Hak

May 1983

**Flow Research Company
A Division of Flow Industries, Inc.
21414-68th Avenue South
Kent, Washington 98032
(206) 872-8500**

Accession For	
NTIS GRA&I	X
DTIC TAB	☐
Unannounced	☐
Justification	

By	
Distribution/	
Availability Codes	
Dist	Avail and/or Special
A	

FOREWORD

On 1 May 1982, Flow Research Company was awarded a one year contract from the Air Force Office of Scientific Research to investigate some unsteady phenomena in boundary layers; in particular, the stability of a decelerating laminar boundary layer. The contract monitor at AFOSR was Captain Michael S. Francis, and the principal investigator at Flow Research was Dr. Mohamed Gad-el-Hak.

The stability of the decelerating laminar boundary layer was investigated experimentally and numerically. The experiments were conducted in an 18-m towing tank, using a flat plate geometry. Flow visualization and probe measurement experiments were conducted. The flow field was visualized and probe measurement experiments were conducted. The flow field was visualized using fluorescent dyes and sheets of argon laser light. The instataneous longitudinal velocity was measured using an array of miniature hot-film probes.

A Blasius boundary layer subjected to uniform deceleration underwent a well-defined route to complete transition. The visualization experiments revealed the onset of two-dimensional waves that appeared after the deceleration had started, three-dimensionality was then apparent and led to the formation of hairpin vortices that lifted away from the wall and burst into turbulence.

The formation and growth of the vorticity waves in the decelerating laminar boundary layer were also observed using hot-film probes. The probes were moved with the plate, and indicated high speed (relative to the plate) fluid coming from the outerparts of the ambient fluid towards the wall region. The probes also indicated a return to the laminar state after the deceleration ceased. The probe measurements indicated the "degree" of two-dimensionality of the vorticity waves observed in the decelerating plate experiment. The waves were truly two-dimensional, and that suggests the study of their instability in order to determine the mechanism and characteristics of the development of three-dimensionality. If there is a well-defined transition from laminar two-dimensional waves to laminar three-dimensional waves through an instability process, one has indentified a major link in the transition process.

The unsteady boundary layer equations were solved numerically to generate instantaneous velocity profiles for a range of boundary and initial conditions. The resulting velocity profiles were inflexional, with the inflexion point initially at the wall. The unsteady flow field was subjected to stability analysis using the Orr-Sommerfeld equation applied to the instantaneous, locally parallel velocity fields. The generalized matrix eigenvalue problem was solved using Chebyshev polynomial spectral methods (QR method).

For profiles at a given station $x = x_0$, the stability calculation shows that the inflexional case has smaller wavelength, smaller phase speed and lower critical Reynolds number than the corresponding Blasius profile. All these trends are consistent with the observations and measurements made. This gives us confidence that the mechanics of the initial instability is well understood. However, the observed appearance of two-dimensional instabilities occurs earlier in the deceleration history than one would predict from the "most dangerous" profile obtained from the stability calculations. In this calculation we used profiles consistent with the measurement station at $x = x_0$. Although one cannot rule out nonlinear effects, the more likely reason for such "earlier" instability is the non-self-similarity of the decelerating boundary layer. Self-similarity of the flow implies that profiles at all stations are "equivalent" in terms of stability characteristics. When the flow is not self-similar, the profiles at different stations are not equivalent, each profile needs to be examined separately and the "most dangerous" station selected. The early appearance of instabilities in the present observations suggest that there are more unstable profiles at neighboring stations whose instabilities propagate to the observation station and are seen before the local profile itself becomes unstable.

In summary then we have both flow visualization and point measurements for the instability and transition processes of flows on decelerating plates. We have obtained theoretical descriptions of the unsteady boundary layer and its instability of two-dimensional <u>laminar</u> waves. These give a consistent picture of the early picture of the early steps of the transition process.

The work on the stability of decelerating laminar boundary layers is a step toward understanding the more complicated problem of the effects of acceleration or deceleration on <u>turbulent</u> boundary layers. This problem has

obvious relevance in accelerating or decelerating vehicles, vehicles experiencing turn and other maneuvers, rotating propellers, and many other practical situations.

On a more basic side, the deceleration experiment offers a convenient way to modulate laminar and turbulent boundary layers; in a way analogous to using pressure gradient, heating or roughness, to help determine the exact nature of the apparent analogies between the different transition events in a laminar boundary layer and the intermittent events that characterize fully-developed turbulent boundary layers, namely the bursting cycle.

Progress to date was presented at the 35th Annual Meeting of the American Physical Society, Division of Fluid Dynamics (Appendix I). A manuscript was submitted to the Journal of Fluid Mechanics and is included with this report as Appendix II. The flow visualization techniques used during this investigation will be presented at the forthcoming Third International Symposium on Flow Visualization. A preprint from the proceedings is given in Appendix III. These publications very much summarize the results of the present investigation and are used in lieu of a final technical report.

1596R

APPENDIX I

Abstract From Bulletin of the American
Physical Society 27, P. 1188, 1982

Physical Review
Analytic Subject Index
Number _____

Bulletin Subject Heading in
which paper should be placed
_____Transition_____

<u>Experimental and Numerical Investigation of the Deceler-
ating Boundary Layer</u>*. M. GAD-EL-HAK and J. T.
MCMURRAY, <u>Flow Research Company</u> -- The stability of a
decelerating boundary layer flow is investigated
experimentally and numerically. Experimentally, a
flat plate having a Blasius boundary layer is decel-
erated in an 18-m towing tank. The boundary layer
becomes unstable to two-dimensional waves which break
down into three-dimensional patterns, hairpin vortices,
and finally turbulent bursts when the vortices lift
off the wall. The unsteady boundary layer equations
are solved numerically to generate instantaneous vel-
ocity profiles for a range of boundary and initial
conditions. A quasi-steady approximation is invoked
and the stability of each velocity profile is deter-
mined by solving the Orr-Sommerfield equation using
Chebyshev matrix methods. The code incorporates a
search algorithm to find the critical Reynolds and
wavenumber for a given eigenvalue and velocity pro-
file. Correlations are made between the numerically
obtained critical Reynolds number and the experiment-
ally observed instabilities.

Submitted by

Signature of APS Member

Flow Research Company
21414 - 68th Avenue South
Kent, WA 98031

Department Name
Institution Name & Address

APPENDIX II

Manuscript Submitted to the
Journal of Fluid Mechanics

On the Stability of the Decelerating
Laminar Boundary Layer

Mohamed Gad-el-Hak

Stephen H. Davis*

J. Thomas McMurray

Steven A. Orszag**

May 1983

Flow Research Company
21414 68th Avenue South
Kent, Washington 98032

*Permanent address: Department of Engineering Science & Applied Mathematics,
Northwestern University, Evanston, IL 60201.

**Permanent address: Department of Mathematics, Massachusetts Institute of
Technology, Cambridge, MA 02139.

Abstract

The stability of a decelerating boundary layer flow is investigated experimentally and numerically. Experimentally, a flat plate having a Blasius boundary layer is decelerated in an 18-m towing tank. The boundary layer becomes unstable to two-dimensional waves which break down into three-dimensional patterns, hairpin vortices, and finally turbulent bursts when the vortices lift off the wall. The unsteady boundary layer equations are solved numerically to generate instantaneous velocity profiles for a range of boundary and initial conditions. A quasi-steady approximation is invoked and the stability of local velocity profiles are determined by solving the Orr-Sommerfeld equation using Chebyshev matrix methods. Comparisons are made between the numerical predictions and the experimentally observed instabilities.

1. Introduction

The classical vehicle for studying shear-flow transition to turbulence consists of a uniform steady flow toward the leading edge of a fixed flat plate. Somewhat downstream of the leading edge a Blasius boundary layer develops. In various stages and in various sequences (to be detailed below) this Blasius layer undergoes small amplitude instability, nonlinear development and transition to turbulence as the displacement-thickness Reynolds number $R_{\delta*}$ increases (Klebanoff, Tidstrom & Sargent, 1962). In effect, $R_{\delta*}$ measures the distance from the leading edge of the plate.

Linearized stability theory can be applied to Blasius profiles treated as locally parallel flows (Lin, 1955; Drazin & Reid, 1981). Squire's (1933) theorem shows that two-dimensional travelling waves, Tollmien-Schlichting waves, are the most dangerous for instability and become unstable when $R_{\delta*}$ exceeds about 520 for long waves having downstream wave number $\alpha* = 0.30$ (Jordinson, 1970). When the above Orr-Sommerfeld theory is modified to take account of non-parallel effects in the boundary layer, the critical $R_{\delta*}$ is reduced to about 420 (Saric & Nayfeh, 1975). However, as soon as nonlinear effects are allowed, three-dimensional disturbances can no longer be excluded.

Observations in experiments having "natural" transition show that clean two-dimensional waves are rarely attainable; rather three-dimensional structure is immediately seen. Efforts to "control" the disturbances have led to the introduction of vibrating ribbons (Klebanoff, Tidstrom & Sargent, 1962) oscillating in ostensibly two-dimensional motions. Although these ribbons are introduced to develop two-dimensional structure, clear three-dimensional fluid motions are still seen. Longitudinal strips of tape have subsequently been introduced to at least fix the spatial structure of this three-dimensional flow (Klebanoff et al., 1962). Given the three-dimensional character of the flow, the road to transition involves amplification of the three-dimensionality, development of "hairpin" vortices and finally the "bursts" of turbulence.

The difficulty in the attainment of purely two-dimensional disturbances and the seeming simultaneous occurrence of both two- and three-dimensional waves has led to several recent attempts at wave-interaction theories (Craik, 1971, 1980; Nayfeh & Bozatli, 1979). Here, Tollmien-Schlichting waves and oblique waves are sought that can lead, through weakly non-linear interactions,

to resonant-like behavior that selects the observed structure prior to bursting. The selection of three-dimensional structure must thus overcome the higher growth rates (Squire's theorem) of the Tollmien-Schlichting waves. Each of these analyses models certain features of the early transition process but no one is completely satisfactory.[*] Finally, there seems to be no theory that is yet capable of the prediction of the hairpin vortices, although there is substantial agreement that intensification of longitudinal vorticity gives rise to locally inflexional (unsteady and three-dimensional) velocity profiles (Stuart, 1965). These profiles seemingly break down (Klebanoff et al., 1962) giving small (spatial) scale features associated with the burst.

An alternative vehicle for the study of the transition process is the decelerating-plate experiment (Fales, 1955; Hegarty, 1958; Davis & Gad-el-Hak, 1981). Here a plate of length L moves steadily normal to its leading edge; L is short enough that the Blasius layer remains laminar along its full length. At time t = 0, the plate is decelerated from a constant initial speed U_o to a new constant final speed U_∞. Flow visualization seemingly shows that a sequence of two-dimensional structures, three-dimensional structures, hairpin vortices and then turbulent bursts results. When the deceleration takes place, the instantaneous velocity profiles are inflexional. If the inviscid instability associated with the instantaneous inflexion point has large enough growth rate, then there is an instability which will cause two-dimensional waves to grow in the unsteady flow (Drazin & Reid, 1981). Subsequently, there is a breakdown (perhaps a new instability of the two-dimensional structure) into three-dimensions, an intensification of the three-dimensional structure, the development of hairpin vortices and then turbulent bursts.

The deceleration experiment differs from the fixed-plate experiment in several respects. First, given the inflexional character of the initial instability, the two-dimensional waves would have substantially larger growth rates than their Tollmien-Schlichting counterparts (Drazin & Reid, 1981). Hence, there may develop a "clean", strongly two-dimensional wave field during the initial stages of the transition process. This contrasts with the mixed two-dimensional - three-dimensional field for the fixed plate experiment (Anders &

---

[*]Orszag & Patera (1983) have shown that a pure two-dimensional structure is prone to strong three-dimensional instabilities.

Blackwelder, 1979). Careful point measurements are required to determine whether this is the case. If this is the case, it suggests the study of this instability in order to determine the mechanism and characteristics of the development of three-dimensionality. The isolation of this problem is one of the main advantages of the deceleration experiment over the fixed-plate experiment. If this picture is correct and there is a well-defined transition from laminar two-dimensional waves to laminar three-dimensional waves through an instability process (Orszag & Patera, 1983), one has identified a major link in the transition process. An understanding of this instability allows one to contemplate means of interferring with the process to delay transition or reinforcing the process to foster transition. It gives one a handle in examining the subsequent evolution to hairpin vortices since these might be examined through the nonlinear evolution of the three-dimensional structure. In summary, the deceleration experiment might be one that clearly separates two-dimensional structures from three-dimensional ones and allows analysis of the change from one to the other.

The present investigation was undertaken to address some of the questions raised above. Experimental and numerical investigations were carried out to determine the mechanics of transition on a decelerating flat plate. A flat plate was towed in the Flow Research 18-m towing tank. Visualization and probe measurements techniques were used to study the different instabilities resulting from decelerating the plate. The unsteady boundary layer equations were solved numerically to generate instataneous velocity profiles for a range of boundary and initial conditions. The stability of such profiles was determined by solving the Orr-Sommerfeld equation using Chebyshev matrix methods.

2. Experimental Equipment and Procedure

2.1 Towing Tank System

· The 18 m long, 1.2 m wide, and 0.9 m deep towing tank and associated equipment have been described by Gad-el-Hak et al. (1981). The flat plate was rigidly mounted under a carriage that rides on two tracks mounted on top of the towing tank. During towing, the carriage was supported by an oil film which insured a vibrationless tow, so that the flow field had an equivalent free-stream turbulence of about 0.1 percent. The carriage was towed with two cables driven through a reduction gear by a 1.5 hp Boston Ratiotrol motor. The towing speed was regulated within an accuracy of 0.1 percent. The main frame supporting the tank could be tilted and levelled by adjusting four screw jacks. This feature was essential for smooth operation of the carriage, whose tracks are supported by the main frame. The towing tank was designed so that flow visualization can be made from the top, sides, bottom and ends. The bottom and side walls are made of 19 mm thick plate glass with optical quality. The end walls are made of 38 mm thick Plexiglas.

2.2 Model and Test Conditions

A unique, modularly designed flat plate was built for the present experiment. Figure 1 is a schematic of the plate, which is 2.7 m long and 1.1 m wide. The working surface is made of Plexiglas and contains two dye slots each with four separate compartments. The working surface is placed on a sheet of 6 mm Plexiglas that is bonded to a 13 mm honeycomb. The NOMEX honeycomb, covered on the bottom side with fiberglass resin, provides buoyancy as well as bending strength. A system of cables and pulleys on the bottom surface insures the flatness of the working surface to within 0.2 mm.

Separation and premature transition at the leading edge is prevented by using a 12:1 elliptic nose and an adjustable lifting flap at the trailing edge. In the range of towing speeds of 20 to 60 cm/sec, a Blasius laminar boundary layer is generated on the working surface.

Uniform deceleration was attained by decreasing the voltage to the Ratiotrol motor. The initial and final speeds were changed in the range of 60 to 0 cm/sec and the deceleration rate varied in the range 1 to 60 cm/sec^2.

2.3 Flow Visualizaton

The transition events were made visible by novel techniques which utilized fluorescent dye, i.e. dye which is visible only when excited by a strong light source of the appropriate wavelength (Gad-el-Hak et al., 1979). This provided an extra degree of freedom in observing the flow because both the dye and light location could be controlled within the limitation of the experimental apparatus. A 5 watt argon laser (Spectra Physics, Model 164) was used with a cylindrical lens to produce a sheet of light that could be projected perpendicular to each of the three axes as required. The light sheets were approximately 1 mm thick, which was sufficient to resolve the large structure within the transitioning and turbulent regions.

Two different methods of dye injection were employed. In the first, a dye sheet seeped into the laminar boundary layer through either of two 0.15 mm wide, 30 cm long spanwise slots located 40 cm and 75 cm downstream of the leading edge. The slots were milled at a 45° angle inclined towards the trailing edge to minimize flow disturbance. Each slot was divided into four separate sections, each with its own dye source, so the spanwise mixing and diffusion of turbulent fluid could be studied. The dye remained on the plate surface until an upward motion caused it to lift. In the second, discrete lines of dye could be allowed to seep into the laminar boundary layer by masking the spanwise slot with a 32 cm long strip of electrical tape, in which thirty longitudinal slots, 1 cm apart and 0.5 cm long, were cut with a surgical knife. The resulting dye lines were less than 0.5 mm wide near the trailing edge of the plate.

2.4 Hot-Film Probes

Miniature hot-film probes, manufactured by Thermo Systems Inc., were used in the present investigation to measure the instantaneous longitudinal velocity before, during and after deceleration. The probe diameter was 0.025 mm and its sensing length was 0.25 mm. The probe support was 0.9 mm diameter and 32 mm long. To obtain a velocity profile, a probe traverse powered with a stepping motor controlled through an APPLE-II microcomputer was used. For data acquisition and analyses, a NOVA 800 and a PRIME 750 minicomputers were used.

3. Analyses

3.1 Theoretical Considerations

3.1.1 Basic State: The Unsteady Boundary Layer

The flow that initially becomes unstable is an unsteady boundary layer caused by plate deceleration. The initial and final states are Blasius layers. Hence, one must solve (Rosenhead, 1963, and Schlichting, 1968):

$$\psi_{yt} + \psi_y\psi_{xy} - \psi_x\psi_{yy} = \psi_{yyy} \tag{1a}$$

$$\psi(x,\infty,t) = 0 \qquad , \ 0 < x < 1 \ , \ t \geq 0 \tag{1b}$$

$$\psi_x(x,0,t) = 0 \qquad , \ 0 < x < 1 \ , \ t \geq 0 \tag{1c}$$

$$\psi_y(x,0,t) = -U_w(t)/U_o \quad , \ 0 < x < 1 \ , \ t \geq 0 \tag{1d}$$

$$\psi(x,y,t) = \psi_B(x,y) \qquad , \ 0 < x < 1 \ , \ t < 0 \ , \ y \geq 0 \tag{1e}$$

Equation (1a) is the non-dimensional longitudinal momentum equation, with the familiar boundary layer approximations applied. In this equation, the downstream coordinate x is non-dimensionalized by L, the normal coordinate y by $L/\sqrt{R}$, the time t by L/U_o, and the stream-function ψ by $U_oL/\sqrt{R}$, where the Reynolds number $R \equiv \frac{U_o L}{\nu}$. Here, $U_w(t)$ is the speed history of the plate, ψ_B signifies the stream-function of the Blasius solution prior to deceleration. The unsteady term in Equatin (1a) makes the boundary layer non-similar.

The unsteady boundary-layer solution of system (1)

$$\psi = \psi(x,y,t) \tag{2}$$

is of a combined Blasius-Rayleigh type (Stewartson, 1951).

3.1.2 Linear Stability Analysis for Locally Parallel Flow

The onset of shear instabilities is obtained by linear stability analysis of the flow (2). Here ψ is unsteady, but one can argue (Davis, 1976) that it is sufficient to examine the "quasi-steady" stability problem in which the instantaneous profiles

$$\psi_s = \psi_s(x,y;t_o) \equiv \psi(x,y,t = t_o) \tag{3}$$

are treated as steady, parallel flows with the Orr-Sommerfeld equation. Such

an approximation is valid if the time rate of change of ψ (measured by a viscous diffusion time) is slow compared to the rate of growth of disturbances of ψ_s (measured by a convection time). This is guaranteed if the steady-flow Reynolds number is sufficiently large. The following Orr-Sommerfeld system defines a critical value of $R_{\delta*}$ for each profile (parameterized by t_o):

$$\left(D^2 - \alpha^2\right)^2 \phi = i \, \bar{R} \left[(\alpha U(y)-\omega)\left(D^2 - \alpha^2\right) \phi - \alpha \frac{d^2 U}{dy^2} \phi \right] , \tag{4a}$$

$$\phi(o) = o , \tag{4b}$$

$$D\phi(o) = o , \tag{4c}$$

$$\phi(\infty) = o , \tag{4d}$$

where we have written the normal modes as follows:

$$\psi(x,y,t) = \phi(y) e^{i(\alpha x - \omega t)} . \tag{5}$$

Here α is the downstream wavenumber and ω is the complex frequency; $D \equiv \frac{d}{dy}$, and $\bar{R}$ is related to the standard displacement thickness Reynolds number $R_{\delta*}$ by:

$$\bar{R} = \sqrt{R} = \sqrt{\frac{U_o L}{\nu}} , \tag{6}$$

$$R_{\delta*} = \bar{R}^2 \frac{U_w}{U_o} \frac{\delta*}{L} . \tag{7}$$

Given that we have used the quasi-steady assumption, Squire's theorem applies and allows us to confine our attention to two-dimensional disturbances only. This is reflected in the form (5).

There is a "most dangerous" profile that corresponds to $t_o = t_{o_c}$; where t_{o_c} is a measure of the time delay between deceleration and the appearance of the first two-dimensional instability. Presumably, the instability is due to the inflexional nature of the profile. Here the point of inflexion at $t = 0$ is at the wall and moves outward on a diffusion time scale. Its location is $y = y_{IP}$; if y_{IP} is too small, viscous effects stabilize the profile. If y_{IP} is too large, the inflexion point is in a region where U is very small so the instability is is not important. The "most dangerous" profile corresponds to an intermediate value of y_{IP} and hence of t_o.

3.2 Numerical Methods

A code was developed to solve the unsteady boundary layer Equation (1) as follows. First, the flow variables are expanded in mapped Chebyshev polynomial expansions. Thus, the variable y is mapped to a new variable Z using:

$$y = S \frac{1+Z}{A-Z} \qquad (-1 \le Z < 1) \qquad (8)$$

where S is a suitable scale parameter. In terms of Z, y derivatives take the form:

$$\frac{\partial F}{\partial y} = \frac{(A-Z)^2}{S(1+A)} \frac{\partial F}{\partial Z} \quad . \qquad (9)$$

Second, the various functions are expanded in Chebyshev polynomial series in Z:

$$F(Z) = \sum_{n=0}^{N} f_n T_n(Z) \ . \qquad (10)$$

Here the nth Chebyshev polynomial $T_n(Z)$ is defined by:

$$T_n(Z) = \cos (n \arccos Z), \qquad (11)$$

for all non-negative integers n (see, e.g. Fox & Parker 1968). Some examples are $T_0(Z) = 1$, $T_1(Z) = Z$, $T_2(Z) = 2Z^2-1$. Also, if F(Z) is represented as in (10), then:

$$F'(Z) = \sum_{n=0}^{N} f_n^{(1)} T_n(Z), \qquad (12)$$

with:

$$f_{n-1}^{(1)} - f_{n+1}^{(1)} = 2nf_n \qquad , \ (n > 1) \ . \qquad (13)$$

Third, the boundary layer equation is solved by discretizing x and t using Crank-Nicolson implicit space and time differencing, in which the difference approximations:

$$\left(\frac{\partial F}{\partial t}\right)_{\left(k+\frac{1}{2}\right)} \Delta t = \frac{F[(k+1)\Delta t]-F(k\Delta t)}{\Delta t} \quad , \qquad (14)$$

$$\left(\frac{\partial F}{\partial x}\right)_{\left(j+\frac{1}{2}\right)} \Delta x = \frac{F[(j+1)\Delta x]-F(j\Delta x)}{\Delta x} \quad , \qquad (15)$$

are used. At the centered points $(j + 1/2)\Delta x$ and $(k + 1/2)\Delta t$, these difference approximations are second-order accurate in both x and t. The fact that (14) and (15) involves functions at the discrete points $(j + 1)\Delta x$ and $(k + 1)\Delta t$ implies that implicit equations must be solved for the dependent variables. These implicit equatins are set up using the Chebyshev derivative matrix operator D defined by:

$$F'(Z_j) = \sum_{n=0}^{N} (Df)_n T_n(Z_j) , \qquad (16)$$

where Z_j are the Chebyshev collocation points:

$$Z_j = \cos \frac{\pi j}{N} . \qquad (17)$$

The resulting equation for the stream-function is nonlinear. This nonlinear equation is solved by quasi-linearization (Newton's method). The resulting iterative scheme is:

$$A = \frac{1}{2\Delta t} D - \frac{1}{2\Delta x} \left[\Psi_y^{(q)}\left(x_j, t_{k+1}\right) D + \frac{1}{4} \left\{ \Psi\left(x_{j+1}, t_k\right) \right. \right.$$
$$\left. + \Psi\left(x_{j+1}, t_{k+1}\right) - \Psi\left(x_j, t_k\right) - \Psi^{(q)}\left(x_j, t_{k+1}\right) \right\} D^2 \right] - D^3$$
$$+ \frac{1}{8\Delta x} \left[\Psi_{yy}\left(x_j, t_k\right) + \Psi_{yy}\left(x_{j+1}, t_k\right) + \Psi_{yy}\left(x_{j+1}, t_{k+1}\right) \right.$$
$$\left. + \Psi_{yy}^{(q)}\left(x_j, t_{k+1}\right) \right] \qquad (18)$$

$$A \left\{ \Psi^{(q+1)}\left(x_j, t_{k+1}\right) - \Psi^{(q)}\left(x_j, t_{k+1}\right) \right\} =$$
$$- \left\{ \left[\Psi_y^{(q)}\left(x_j, t_{k+1}\right) + \Psi_y\left(x_{j+1}, t_{k+1}\right) - \Psi_y\left(x_j, t_k\right) - \Psi_y\left(x_{j+1}, t_k\right) \right] \frac{1}{2\Delta t} \right.$$
$$+ \left[\Psi_y\left(x_{j+1}, t_k\right)^2 + \Psi_y\left(x_{j+1}, t_{k+1}\right)^2 - \Psi_y\left(x_j, t_k\right)^2 - \Psi_y^{(q)}\left(x_j, t_{k+1}\right)^2 \right.$$
$$- \frac{1}{2} \left(\Psi\left(x_{j+1}, t_k\right) + \Psi\left(x_{j+1}, t_{k+1}\right) - \Psi\left(x_j, t_k\right) - \Psi^{(q)}\left(x_j, t_{k+1}\right) \right) \times$$
$$\left. \left(\Psi_{yy}\left(x_{j+1}, t_k\right) + \Psi_{yy}\left(x_j, t_k\right) + \Psi_{yy}\left(x_{j+1}, t_{k+1}\right) + \Psi_{yy}^{(q)}\left(x_j, t_{k+1}\right) \right) \right] \frac{1}{4\Delta x}$$
$$\left. - \Psi_{yyy}^{(q)}\left(x_j, t_{k+1}\right) \right\} \qquad (19)$$

Typically, only a few iterations are necessary to converge. The advantage of this method is that it is unconditionally stable.

At the inflow location x_0, Blasius flow is imposed. The Blasius equation is solved by the Chebyshev spectral scheme outlined above, also using Newton's method.

At each downstream location, the flow field can be subjected to stability analysis using the Orr-Sommerfeld equation applied to the instantaneous velocity profile. The Orr-Sommerfeld system (4) is solved using Chebyshev polynomial spectral methods on the same Z_j grid described above. The Chebyshev approximations permit simulations of very high accuracy. The Orr-Sommerfeld eigenvalue problem for temporally unstable mode is formulated as a generalized matrix eigenvalue problem of the form:

$$A \, \phi = \lambda B \, \phi \ . \tag{20}$$

The eigenvalues of the resulting matrix problem are found by first reducing the problem (20) (with a singular matrix B) to a standard eigenvalue problem of the form $Ax = \lambda x$ with scalar λ and then finding the eigenvalues of this problem using the QR method (Orszag, 1971). If a good guess for an eigenvalue is available, then the code is able to avoid the global QR computation by using a local inverse Rayleigh iteration method to efficiently improve the guess. In all cases, the matrix method is designed so that the only unstable modes that are computed (either globally or locally) are approximations to physical modes; there are no spurious unstable modes. This feature is achieved by writing Orr-Sommerfeld equation in such a form that the numerical method would give a stable forward time-integration method for the linearized Navier-Stokes equations, so spurious unstable modes (that would lead to numerical instablity in time) cannot be present.

The code also has the optional features of obtaining the minmum critical Reynolds number at a given x-station and the neutral curve at the given x-station. These computations are done using variants of Newton's method. Thus, quick convergence of a guess to the neutral curve $\mathrm{Im}\ \omega = 0$ is gotten by the iterative method:

$$\omega = \omega\!\left(\alpha_n, \bar{R}_n\right) \ , \tag{21}$$

$$\alpha_{n+1} = \alpha_n - \frac{\text{Im } \omega \cdot \frac{\partial \text{ Im } \omega}{\partial \alpha}}{\left(\frac{\partial \text{ Im } \omega}{\partial \alpha}\right)^2 + \left(\frac{\partial \text{ Im } \omega}{\partial \bar{R}}\right)^2} \quad , \tag{22}$$

$$\bar{R}_{n+1} = \bar{R}_n - \frac{\text{Im } \omega \cdot \frac{\partial \text{ Im } \omega}{\partial \bar{R}}}{\left(\frac{\partial \text{ Im } \omega}{\partial \alpha}\right)^2 + \left(\frac{\partial \text{ Im } \omega}{\partial \bar{R}}\right)^2} \quad . \tag{23}$$

Once one point on the neutral curve is obtained, additional points on it are obtained by using as a first guess a point of the form:

$$\hat{\alpha} = \alpha + q \frac{\partial}{\partial \bar{R}} \text{ Im } \omega \quad , \tag{24}$$

$$\hat{\bar{R}} = \bar{R} - q \frac{\partial}{\partial \alpha} \text{ Im } \omega \quad , \tag{25}$$

which is obtained by moving along the tangent to the neutral curve at the computed point.

The minimum critical Reynolds number program also uses Newton's method. Here the iterative equations are:

$$\alpha_{n+1} = \alpha_n + \Delta\alpha \quad , \tag{26}$$

$$\bar{R}_{n+1} = \bar{R}_n + \Delta R \quad , \tag{27}$$

$$\text{Im } \omega\left(\alpha_n, \bar{R}_n\right) + \frac{\partial}{\partial \alpha} \text{ Im } \omega\left(\alpha_n, \bar{R}_n\right)\Delta\alpha + \frac{\partial}{\partial \bar{R}} \text{ Im } \omega\left(\alpha_n, \bar{R}_n\right)\Delta R = 0 \quad , \tag{28}$$

$$\frac{\partial}{\partial \alpha} \text{ Im } \omega\left(\alpha_n, \bar{R}_n\right) + \frac{\partial}{\partial \alpha^2} \text{ Im } \omega\left(\alpha_n, \bar{R}_n\right)\Delta\alpha + \frac{\partial^2}{\partial \alpha \, \partial \bar{R}} \text{ Im } \omega\left(\alpha_n, \bar{R}_n\right)\Delta R = 0 \quad . \tag{29}$$

In summary, the above described code uses an unconditionally stable, spectral, accurate integration program for the solution of the time-dependent non-self-similar boundary layer equations and both global and local spectral methods for the solution of the Orr-Sommerfeld equation. The code is reasonably robust, having significant difficulty only in cases when the flow reverses.

4. Results and Discussion

4.1 Flow Visualization Results

When the Blasius boundary layer was subjected to a uniform deceleration, a most interesting series of events was observed. Figure 2 represents six selected frames from a movie of the observed instabilities. The left-hand side of each frame was at x = 92 cm, and the right-hand side was at x = 108 cm. Fluorescent dye seeped into the laminar boundary layer through the spanwise slot, and was illuminated by a horizontal sheet of laser light at y = 0. The thickness of the laser sheet was about 1 mm, several times the thickness of the undisturbed dye sheet. At a uniform speed of 40 cm/sec the boundary layer was of Blasius type (see Section 4.2), and the dye sheet appeared smooth and uniform as shown in Figure 2a. The plate was then decelerated uniformly to a speed 30 cm/sec in 5 seconds. Two seconds after the deceleration had started, the two-dimensional pattern depicted on Figure 2b was evident. The alternating bright and dark bands are consistent with the passing of two-dimensional vorticity waves. The wavelength of the disturbance was about 5 to 6 boundary layer thicknesses δ as compared to a wavelength 8δ for a *Tollmien-Schlichting* wave occurring in a non-decelerating Blasius boundary layer having the same Reynolds number. The wave phase-speed relative to the plate was about 10 cm/sec as compared to 14 cm/sec for the corresponding Tollmien-Schlichting wave. The two-dimensional waves developed a three-dimensional pattern as shown on Figure 2c. This pattern evolved into several hairpin vortices characterized by the bright triangles in Figure 2d. Since the thickness of the sheet of light is larger than the thickness of the undisturbed dye, bright regions indicate lifting and accumulation of dye. The vortices appeared in several regular rows with a spanwise distance between two vortices of about 5δ (or about the same as the wavelength of the two-dimensional waves). The patterns continued to convect towards the trailing edge of the plate, and new ones appeared near the leading edge. Side views of the hairpin vortices indicated that their heads moved away from the wall. When the vortex head reached a height of about half a boundary layer thickness, it then burst into turbulence as shown in Figure 2e. The turbulent regions grew in size as shown in Figure 2f, and adjacent bursts coalesced. Shortly afterward, the dye pattern indicated that the flow over the entire plate was turbulent.

The experiments where repeated with different initial velocities in the range 20 to 60 cm/sec and different deceleration rates in the range 1 to 60 cm/sec^2. The same sequence of events described above was observed in all runs. The length scales were not sensitive to the changes in the deceleration rate. However, the time to complete the transition process was approximately inversely proportional to the deceleration rate. The stages of transition are summarized in the schematic depicted in Figure 3.

To gain more physical insight into the transition process in the decelerating boundry layer, the above described sequence of events was also observed using discrete lines of dye embedded into the laminar boundary layer (Section 2.3). Figure 4 shows six selected frames from a movie of a typical run. Before decelerating the flat plate, the dye streaks were parallel to the flow and remained on the plate surface. The plate was then decelerated from a speed 40 cm/sec to a speed 30 cm/sec in 5 seconds. A short time after the deceleration had started, the two-dimensional waves with their fronts perpendicular to the dye streaks appeared as alternating bright and dark bands on each streak as shown in Figure 4a. The waves moved in the same direction, relative to the plate, as the ambient fluid. As the amplitude of these two-dimensional waves increased, as evident by the intensification of the contrast between the bright and dark bands, three-dimensionality developed, the dye lines began to show a waviness that has the same wavelength as that of the original two-dimensional waves (Figures 4b and 4c). Liepmann, Brown and Nosenchuck (1982), in observing a somewhat similar transition process initiated by a dynamic-heating technique, speculated that the waviness of the dye lines indicates a local development of longitudinal vorticity corresponding with the local warping of the initially parallel vortex lines. The dye became concentrated in regions that has been lifted away from the wall into a higher-velocity region of the boundary layer, thereby catching up with that released at an earlier time. The transition process continued as before until the dye pattern indicated turbulent flow over the entire plate (Figures 4d-4f).

4.2 Hot-Film Probe Measurements

Miniature hot-film probes were used to measure the instantaneous longitudinal velocity in the decelerating boundary layer. The probes were moved

with the plate, so that all velocities recorded were relative to the plate. Before the deceleration started, the boundary layer was of Blasius type as shown on Figure 5. The velocity profiles are plotted in the normal boundary layer coordinates, where the ambient speed U_o is used as a velocity scale and the length scale $\sqrt{\frac{\nu x}{U_o}}$ is proportional to the laminar boundary layer thickness δ. The Reynolds number for the two runs shown on Figure 5 was $\frac{U_o x}{\nu} = 6.7 \times 10^5$ ($R_{\delta*} = 1400$). The solid line in the figure is a numerically generated Blasius profile.

Figure 6 represents the instantaneous longitudinal velocity $U(y)$ at $y/\delta = 0.1$, for a plate decelerated from an initial velocity $U_o = 40$ cm/sec to a final velocity $U_\infty = 32$ cm/sec in a time $t^* = 4.6$ seconds. The two arrows on the abscissa represent the starting and ending of deceleration. Initially, the flow is laminar and the velocity at this particular elevation is proportional to the towing speed. A short time[*] after the deceleration starts, a sinusoidal instability is observed. Its peak to peak amplitude grows rapidly as shown in Figure 6. Characteristic turbulent fluctuations are then observed, followed by a return to the laminar state when the plate is again moving at its new constant towing speed. The turbulence, on the average, brings high speed fluid from outside the boundary layer to replace the low speed fluid near the wall. A second probe at $y/\delta = 1$ recorded the signal shown in Figure 7. It is seen that the turbulent fluctuations, on the average, bring low speed fluid from the wall region to replace the high speed fluid at $y/\delta = 1$. Close inspection of the instability waves near the wall and away from the wall reveals that the two wave trains are out of phase, consistent with a spanwise vortical motion.

The instability waves appeared from the visualization experiments to be two-dimensional initially. To check the "degree" of two-dimensionality of these vorticity waves, three hot-film probes were located at $y/\delta = 0.1$ at the same streamwise position $x/L = 0.8$, with a spanwise separation of two boundary layer thicknesses. The plate was decelerated from 40 cm/sec to 30 cm/sec in 5 seconds. The streamwise velocity signals from all three probes are plotted in

---

[*]The exact delay time between the start of deceleration and the onset of instability is difficult to determine, since the observed waves are infinitesimal at first.

Figure 8. The waves are quite two-dimensional, although they have grown to relatively very large amplitude. Thus, the development of a "clean," two-dimensional wave field during the initial stages of the transition process on the decelerating flat plate contrasts with the mixed two-dimensional/three-dimensional field for the fixed plate experiment (Anders & Blackwelder, 1979).

The probe measurements are consistent with the qualitative visualization experiments. The "relaminization" observed in the hot-film signal after the plate returns to a uniform speed does not show in the dye pictures, however, since the dye delineates the regions of the flow which have been marked by it, and at any instant of time it mainly gives information which is time-integrated over the history of the flow from the time of release of the dye.

4.3 Numerical Results

The unsteady-boundary-layer system (1) was solved by expanding the flow variables (dependence on y) in mapped Chebyshev polynomal expansions, and discretizing x and t using Crank-Nicolson implicit space and time differencing. The code uses an unconditionally stable, spectral, accurate integration program for the solution of the time-dependent non-self-similar boundary layer equations. The code is reasonably robust, having significant difficulty only in cases when the flow reverses so the boundary-layer approximation is not valid.[*] This occured for deceleration rates larger than 4 cm/sec^2.

The resulting velocity profiles for a typical deceleration rate are presented in Figure 9. Here, the initial and final speeds were 40 and 22.5 cm/sec, respectively, and the deceleration rate was 3.5 cm/sec^2. At t=0, the velocity profile is of (inverted) Blasius type with the inflexion point at y=0. The subsequent velocity profiles are inflexional, with the point of inflexion moving away from the wall on a viscous-diffusion-time scale. At large times, a new Blasius profile is established after the inflexional point returns back to the wall.

The unsteady boundary layer equation was solved for a range of initial and boundary conditions comparable to the experimental runs. Since the solution is non-self-similar, it is obtained at selected streamwise locations. The migration of the inflexion point for seven different deceleration rates is shown in

---

[*]Flow reversal changes the parabolic partial differential equation to an elliptic one requiring both inflow and outflow boundary conditions.

Figure 10. The position $y_{IP}(t)$ of the inflexion point is normalized with the length scale $\dfrac{L}{\sqrt{R}}$, and the time t is normalized with the deceleration time t*. The initial speed was U_0 = 40 cm/sec, and the plate was decelerated in a time t* = 5 seconds to a final speed U_∞ = 37.5, 35.0, 32.5, 30.0, 27.5, 25.0 and 22.5 cm/sec. The dip in the curve corresponding to a final speed U_∞ = 22.5 cm/sec is an indication of the incipient breakdown of the numerical simulation as mentioned above. The inflexion point migrates farther from the wall for high deceleration rate. It reaches a particular position above the wall in a time that is inversely proportional to the deceleration rate. This is consistent with the experimental observation that transition occurs sooner for higher deceleration rates, provided that there is a "most dangerous" location above the wall for the inflexion point.

The flow field resulting from solving the unsteady boundary-layer equation was then subjected to stability analysis using the Orr-Sommerfeld equation applied to the instantaneous velocity profiles. The linear stability equation was solved using Chebyshev polynomial spectral methods (Orszag, 1971). As expected, the inflexional velocity profiles yielded lower critical Reynolds numbers and larger growth rates in the unstable region as compared to the Blasius profile. The neutral stability curves during a typical deceleration are depicted in Figure 11a, and enlarged in Figure 11b. The plate was decelerated from an initial speed 40 cm/sec to a final speed 30 cm/sec in 5 seconds. At t=0, the neutral stability curve for a Blasius profile resulted. As the plate decelerates, the inflexion point migrates away from the wall and the neutral stability curve moves toward the left, reaching its foremost left position at the end of the deceleration period (t=5 sec). Note that the inflexion point for this run reaches its maximum distance from the wall at t = 6.25 sec (see Figure 10). Finally, the inflexion point moves toward the wall and the neutral stability curve moves back toward the neutral curve of the Blasius profile. The unstable modes for the inflexional velocity profiles tend to have larger wavenumbers (smaller wavelengths) as compared to the unstable modes for a Blasius velocity profile.

The critical Reynolds number for a particular velocity profile is the smallest value of Reynolds number for which an unstable eigenmode exists. The behavior of the critical Reynolds number for seven different deceleration rates

is shown in Figure 12. The critical Reynolds number R_c is normalized with the critical Reynolds number for a Blasius velocity profile $(R_c|_{Blasius} = 520)$, and the time t is normalized with the deceleration time t*. The plate was decelerated from an initial speed $U_o = 40$ cm/sec to a final speed $U_\infty = 37.5$, 35.0, 32.5, 30.0, 27.5, 25.0 or 22.5 cm/sec in a time t* = 5 seconds. The critical Reynolds number decreases with time then tends back to the Blasius value as the inflexion point migrates back toward the wall. The lowest critical Reynolds number decreases as the deceleration rate increases, and occurs at t/t* = 1. For a deceleration rate of 3.5 cm/sec^2, the lowest critical Reynolds number is about 20% of the corresponding Blasius value.

The critical Reynolds number indicates qualitatively the "degree" of instability for a particular experimental condition, where the actual Reynolds number usually far exceeds the critical one. For a certain decelerating boundary layer, the Reynolds number changes with time at a prescribed streamwise location on the plate. Of particular interest to the experiment is then to determine, at a particular location on the plate, the most unstable mode at each instant of time. Vertical scans of the stability diagrams were conducted at the experimental Reynolds number at x = 160 cm, corresponding to a typical observation station. The results are depicted in Figures 13 through 16.

The imaginary part of the eigenvalue ω_i indicates the exponential growth (or damping) of the disturbance amplitude. Figure 13 shows the growth rate ω_i versus wavelength $\lambda \left(\equiv \frac{2\pi}{\alpha}\right)$ for the unstable modes as a plate is decelerated from 40 cm/sec to 30 cm/sec in 5 sec. It is seen that, for each velocity profile, there exists a "most-dangerous" wavelength corresponding to the maximum growth rate. As time increases, this most-dangerous wavelength decreases slightly. This is consistent with the experimental observation (Section 4.1) that the observed wavelength in the present decelerating plate experiment is shorter than the Tollmein-Schlichting wave in a Blasius boundary layer. In particular, at t = 5 sec, the most-dangerous wavelength is about 6.5 cm, whereas at t=0, it is 8 cm. The computations were repeated for a plate decelerated from 40 cm/sec to 25 cm/sec and 35 cm/sec in 5 sec. The most dangerous wavelength at the end of the deceleration period varied in the range of 5 to 7 cm, decreasing as the deceleration rate increased. This relative insensitivity of the length scale to changing the deceleration rate was observed in the flow visualization experiments (Section 4.1).

Unlike the wavelength, the growth rate of the disturbance depends strongly on the deceleration rate. The maximum growth rate during deceleration for all three deceleration rates (1, 2 and 3 cm/sec^2) is shown in Figure 14. It increases as the deceleration takes place reaching a maximum at the end of the deceleration period t = 5 sec, then declines moving back towards the Blasius value. At a particular time during the deceleration, the growth rate increases as the deceleration rate increases. At the end of the deceleration period, the maximum growth rate for a plate decelerated to a final speed U_∞ = 25, 30 and 35 cm/sec is about 5, 4 and 2 times, respectively, that for a Blasius velocity profile.

The real part of the eigenvalue ω_r is proportional to the phase velocity of the two-dimensional disturbance $c_p \left(\equiv \frac{\omega_r}{\alpha} \right)$. Figure 15 shows the phase velocity versus wavelength for the unstable modes for different times during a deceleration from 40 cm/sec to 30 cm/sec in 5 sec. For a particular wavelength, the phase velocity decreases as the plate is decelerated, reaching a minimum at the end of the deceleration period. The phase velocity for the most-amplified disturbance during deceleration is shown in Figure 16, for three deceleration rates 1, 2 and 3 cm/sec^2. Consistent with the flow visualization results, the phase velocity for the inflexional velocity profiles is less than that for the Blasius boundary layer. For a plate decelerated to a final speed 25, 30 and 35 cm/sec and at the end of the deceleration period (t = 5 sec), the phase velocity for the most-amplified disturbance is 63, 74 and 87 percent, respectively, of that for a Blasius velocity profile.

5. Concluding Remarks

The stability of the decelerating laminar boundary layer was investigated experimentally and numerically. The experiments were conducted in an 18-m towing tank, using a flat plate geometry. Flow visualization and probe measurement experiments were conducted. The flow field was visualized using fluorescent dyes and sheets of argon laser light. The instantaneous longitudinal velocity was measured using an array of miniature hot-film probes.

A Blasius boundary layer subjected to uniform deceleration underwent a well-defined route to complete transition. The visualization experiments revealed the onset of two-dimensional waves that appeared after the deceleration had started, three-dimensionality was then apparent and led to the formation of hairpin vortices that lifted away from the wall and burst into turbulence.

The formation and growth of the vorticity waves in the decelerating laminar boundary layer were also observed using hot-film probes. The probes were moved with the plate, and indicated high speed (relative to the plate) fluid coming from the outerparts of the ambient fluid towards the wall region. The probes also indicated a return to the laminar state after the deceleration ceased. The probe measurements indicated the "degree" of two-dimensionality of the vorticity waves observed in the decelerating plate experiment. The waves were truly two-dimensional, and that suggests the study of their instability in order to determine the mechanism and characteristics of the development of three-dimensionality. If there is a well-defined transition from laminar two-dimensional waves to laminar three-dimensional waves through an instability process, one has identified a major link in the transition process.

The unsteady boundary layer equations were solved numerically to generate instantaneous velocity profiles for a range of boundary and initial conditions. The resulting velocity profiles were inflexional, with the inflexion point initially at the wall, moving upward on a diffusion time scale and finally going back to the wall. The unsteady flow field was subjected to stability analysis using the Orr-Sommerfeld equation applied to the instantaneous, locally parallel velocity fields. The generalized matrix eigenvalue problem was solved using Chebyshev polynomial spectral methods (QR method).

For profiles at a given station $x = x_o$, the stability calculation shows that the inflexional case has smaller wavelength, smaller phase speed and lower critical Reynolds number than the corresponding Blasius profile. All these trends are consistent with the observations and measurements made. This gives us confidence that the mechanics of the initial instability is well understood. However, the observed appearance of two-dimensional instabilities (say, in a 5 sec deceleration run) occurs earlier in the deceleration history (e.g. at $t \simeq 2$ sec) than one would predict from the "most dangerous" profile obtained from the stability calculations (for which one would have $t = 5$ sec). In this calculation we used profiles consistent with the measurement station at $x = x_o$. Although one cannot rule out nonlinear effects, the more likely reason for such "earlier" instability is the non-self-similarity of the decelerating boundary layer. Self-similarity of the flow implies that profiles at all stations are "equivalent" in terms of stability characteristics. When the flow is not self-similar, the profiles at different stations are not equivalent, each profile needs to be examined separately and the "most dangerous" station selected. The early appearance of instabilities in the present observations suggests that there are more unstable profiles at neighboring stations whose instabilities propagate to the observation station and are seen before the local profile itself becomes unstable.

In summary then we have both flow visualization and point measurements for the instability and transition processes of flows on decelerating plates. We have obtained theoretical descriptions of the unsteady boundary layer and its instability to two-dimensional laminar waves. These give a consistent picture of the early steps of the transition process.

The work on the stability of decelerating laminar boundary layers is a step toward understanding the more complicated problem of the effects of acceleration or deceleration on turbulent boundary layers. This problem has obvious relevance in accelerating or decelerating vehicles, vehicles experiencing turn and other maneuvers, rotating propellers, and many other practical situations.

On a more basic side, the deceleration experiment offers a convenient way to modulate laminar and turbulent boundary layers; in a way analogous to using pressure gradient, heating or roughness, to help determine the exact nature of

the apparent analogies between the different transition events in a laminar boundary layer and the intermittent events that characterize fully-developed turbulent boundary layers, namely the bursting cycle.

References

Anders, J. B., and Blackwelder, R. F., (1979) "Longitudinal Vortices in a Transitioning Boundary Layer," Proc. IUTAM Symp. on Laminar-Turbulent Transition, University of Stuttgart, p. 110.

Craik, A. D. D., (1971) "Non-Linear Resonant Instability in Boundary Layers," J. Fluid Mech. 50, p. 393.

Craik, A. D. D., (1980) "Nonlinear Evolution and Breakdown in Unstable Boundary Layers," J. Fluid Mech. 99, p. 247.

Davis, S. H., (1976) "The Stability of Time-Periodic Flows," Ann. Rev. Fluid Mech. 8, p. 57.

Davis, S. H., and Gad-el-Hak, M., (1981) "Transition in Decelerating Boundary Layers," Bull. Amer. Phys. Soc. 26.

Drazin, P., and Reid, W., (1981) Hydrodynamic Stability, Cambridge University Press.

Fales, E. N., (1955) "A New Laboratory Technique for Investigation of the Origin of Fluid Turbulence," J. Franklin Inst. 259, p. 491.

Fox, L., and Parker, I. B., (1968) "Chebyshev Polynomials in Numerical Analysis," Oxford Univ. Press.

Gad-el-Hak, M., Blackwelder, R. F., and Riley, J. J., (1979) "A Visual Study of the Growth and Entrainment of Turbulent Spots," Proc. IUTAM Symp. on Laminar-Turbulent Transiton, Univ. Stuttgart, p. 297.

Gad-el-Hak, M., Blackwelder, R. F., and Riley, J. J., (1981) "On the Growth of Turbulent Regions in Laminar Boundary Layers," J. Fluid Mech. 110, p. 73.

Hegarty, J. C., (1958) "Investigation of Transition Caused by the Stopping of a Flat Plate," AFOSR TN58-627.

Herbert, Th. (1976) "Periodic Secondary Motions in Plane Channel Flow," Proc. Fifth Int. Conf. on Numerical Methods in Fluid Dynamics, Springer, p. 235.

Jordinson, R. (1970) "The Flat Plate Boundary Layer. Part 1: Numerical Integration of the Orr-Sommerfeld Equation," J. Fluid Mech. 43, p. 801.

Klebanoff, P. S., Tidstrom, K. D., and Sargent, L. M. (1962) "The Three-Dimensional Nature of Boundary Layer Instability," J. Fluid Mech. 12, p. 1.

Liepmann, H. W., Brown, G. L., and Nosenchuck, D. M. (1982) "Control of Laminar - Instability Waves Using a New Technique," J. Fluid Mech. 118, p. 187.

References (Cont.)

Lin, C. C. (1955) <u>The Theory of Hydrodynamic Stability</u>, Cambridge University Press.

Nayfeh, A. H., and Bozatli, A. N. (1979) "Nonlinear Wave Interactions in Boundary Layers," AIAA 12th Fluid & Plasma Dyn. Conf., Williamsburg, Paper 79-1496.

Orszag, S. A. (1971) "Accurate Solution of the Orr-Sommerfeld Stability Equation," <u>J. Fluid Mech.</u> <u>50</u>, p. 689.

Orszag, S. A., and Patera, A. T. (1983) "Secondary Instability of Wall-Bounded Shear Flows," <u>J. Fluid Mech.</u> <u>128</u>, p. 347.

Rosenhead, L. (1963) <u>Laminar Boundary Layers</u>, Oxford Clarendon Press.

Saric, W. S., and Nayfeh, A. H. (1975) "Nonparallel Stability of Boundary-Layer Flows," <u>Phys. Fluids</u> <u>18</u>, p. 945.

Schlichting, H. (1968) <u>Boundary Layer Theory</u>, McGraw-Hill.

Squire, H. B. (1933) "On the Stability of Three-Dimensional Disturbances of Viscous Flow between Parallel Walls," <u>Proc. Roy. Soc. A</u> <u>142</u>, p. 621.

Stewartson, K. (1951) "On the Impulsive Motion of a Flat Plate in a Viscous Fluid," <u>Quat. J. Mech.</u> <u>4</u>, p. 182.

Stuart, J. T. (1965) "The Production of Intense Shear Layers by Vortex Stretching and Convection," AGARD Report 514.

Zahn, J. P., Toomre, J., Spiegel, E. A., and Gough, D. O. (1974) "Nonlinear Cellular Motions in Poiseuille Channel Flow," <u>J. Fluid Mech.</u> <u>64</u>, p. 319.

List of Figures

Figure 1. Schematic of the Flat Plate and Co-ordinate System

a

FLOW
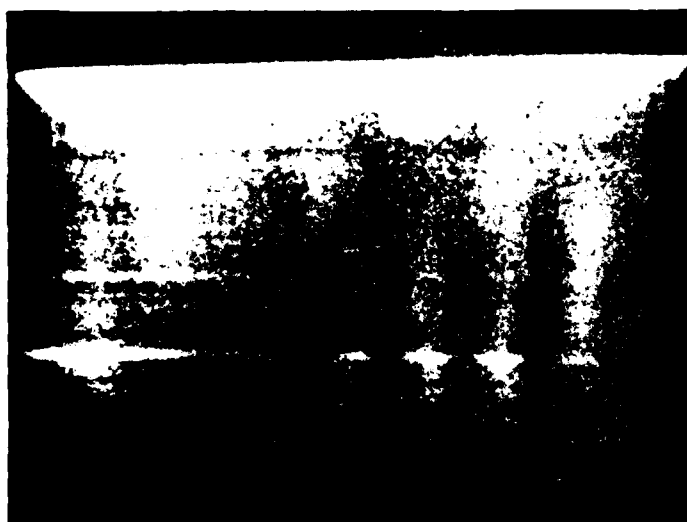
b

Figure 2. Instabilities in a Decelerating Boundary Layer
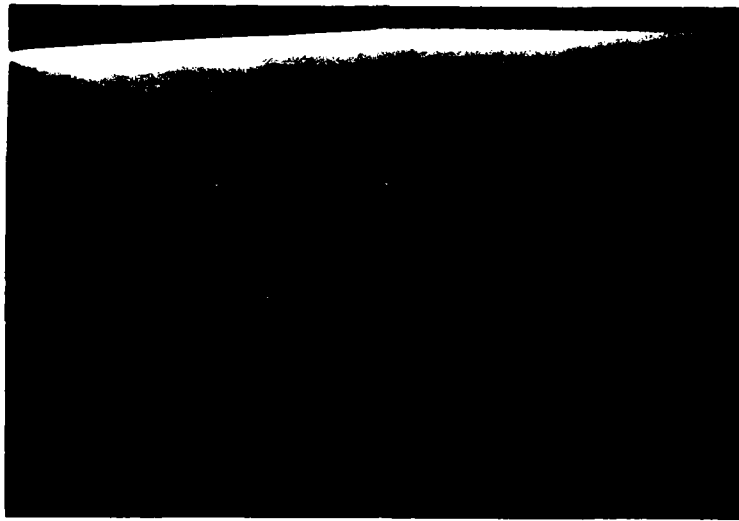
c

FLOW

d

Figure 2.   Instabilities in a Decelerating Boundary Layer (Cont.)
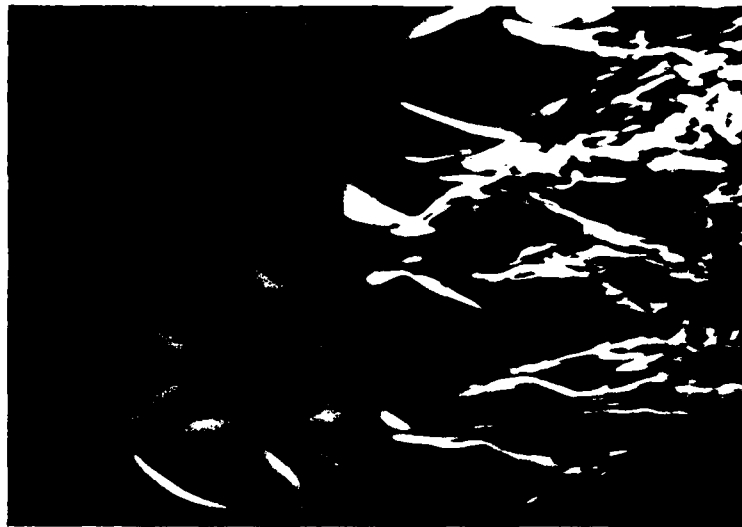
e

FLOW
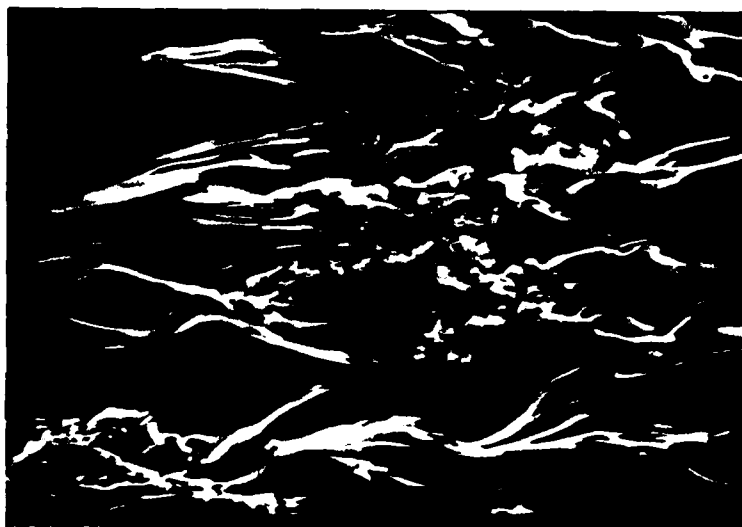
f

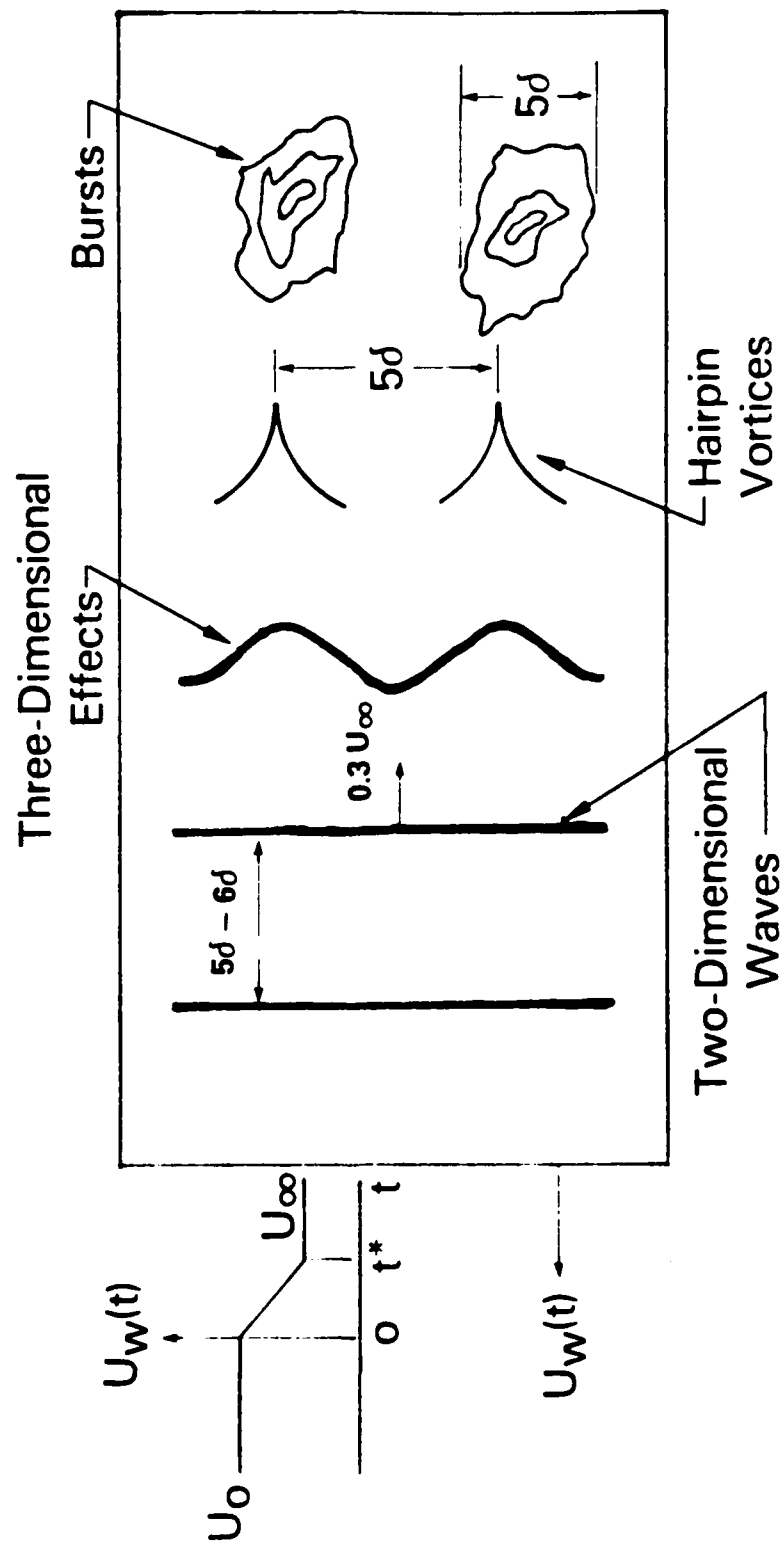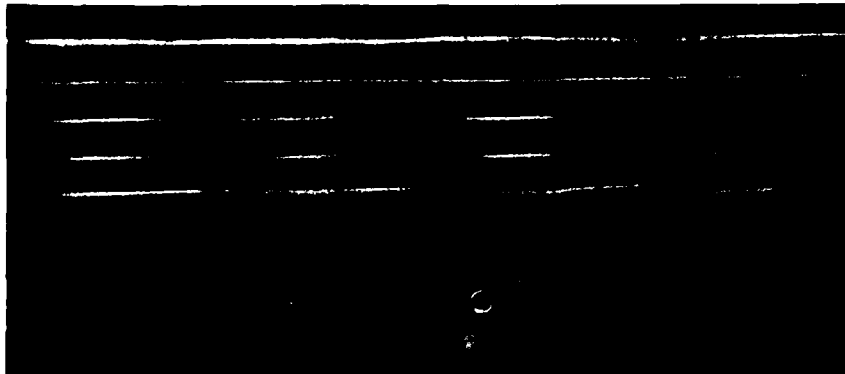Figure 2. Instabilities in a Decelerating Boundary Layer (Cont.)

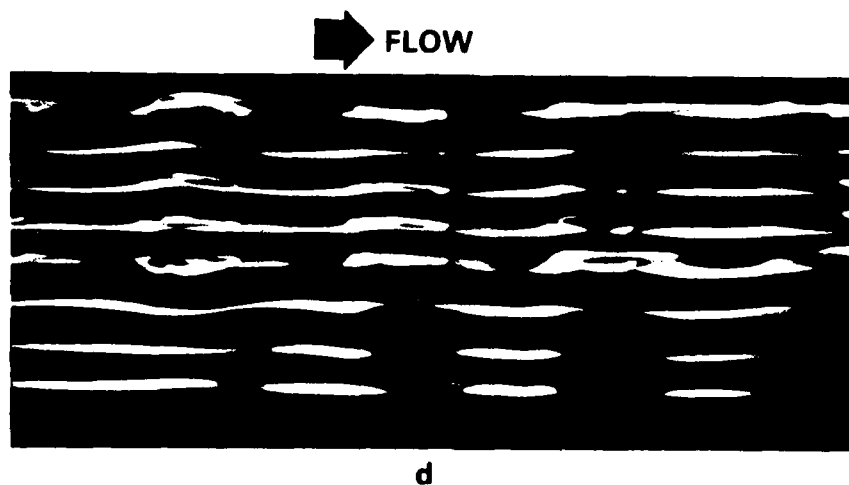Figure 3.   Schematic of Transition Events in a Decelerating Boundary Layer
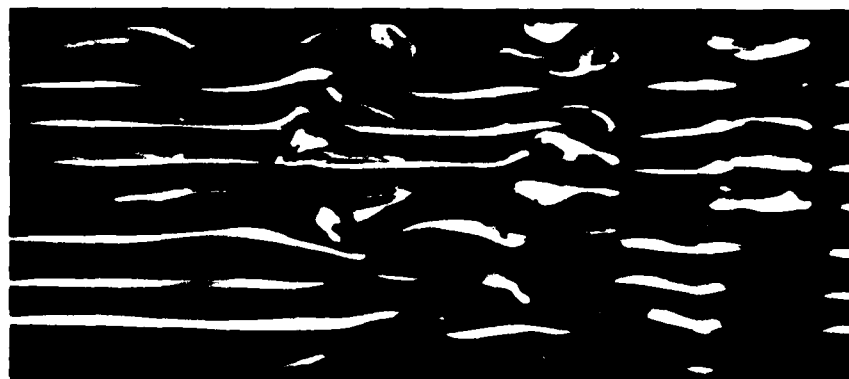
FLOW

a

b

c

Figure 4. Dye-Streaks Visualization During Deceleration

FLOW

d

e

f

Figure 4. Dye-Streaks Visualization During Deceleration (Cont.)

$$R_x = 6.7 \times 10^5$$

—— Blasius Profile

$\dfrac{y}{\sqrt{\dfrac{\nu x}{U_o}}}$

U/U_o
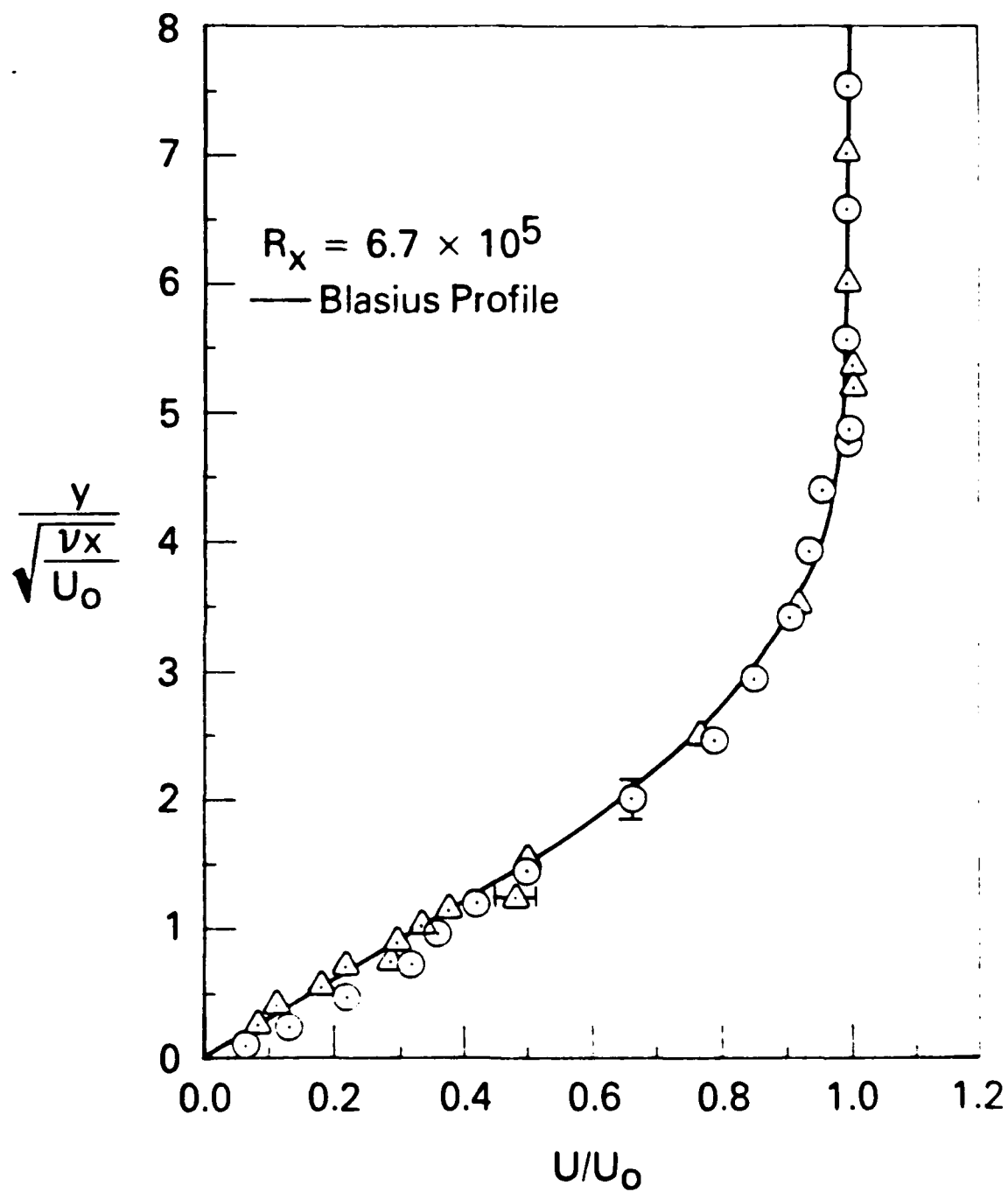
Figure 5. Laminar Boundary Layer Profiles
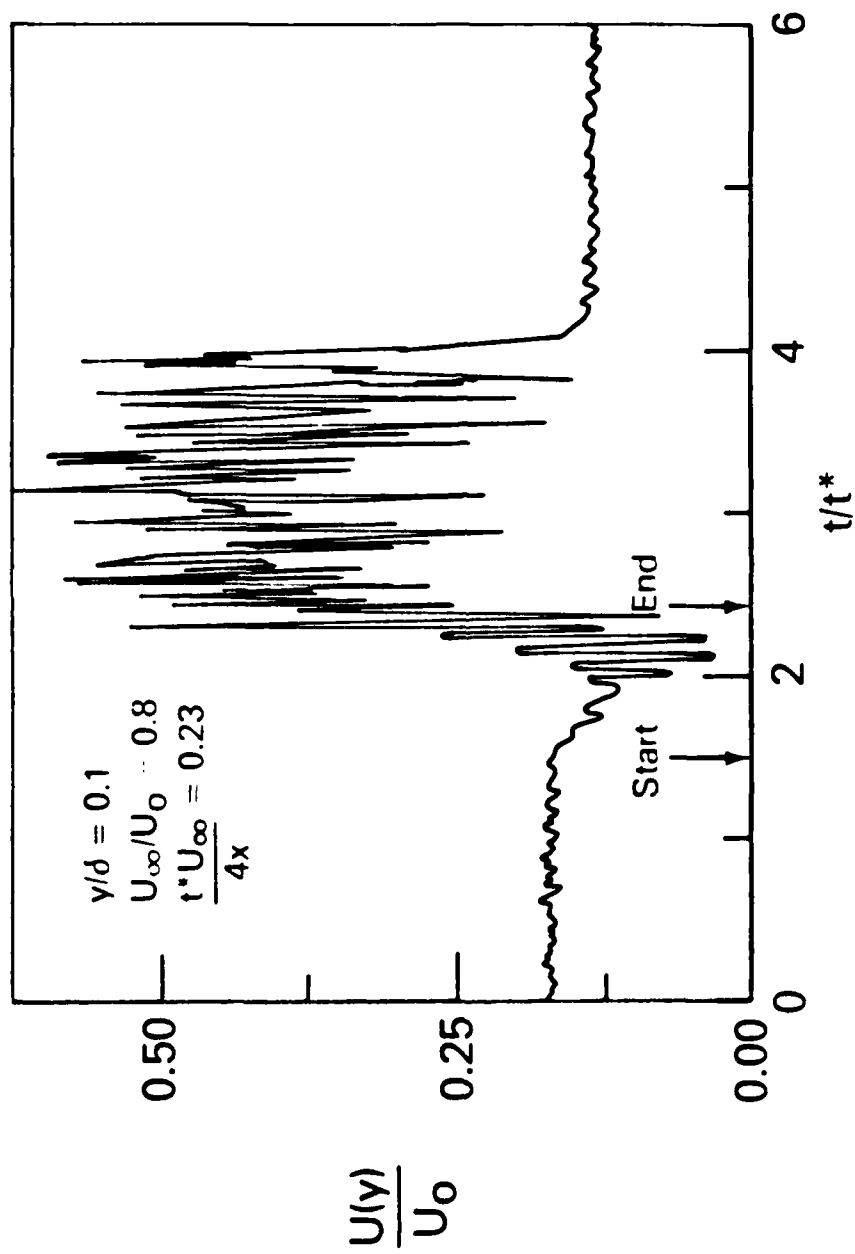
Figure 6.   Longitudinal Velocity Near the Wall

$y/\delta = 1.0$
$U_\infty/U_o = 0.8$
$\dfrac{t^* U_\infty}{4x} = 0.23$

Start

End

$\dfrac{U(y)}{U_o}$

t/t^*
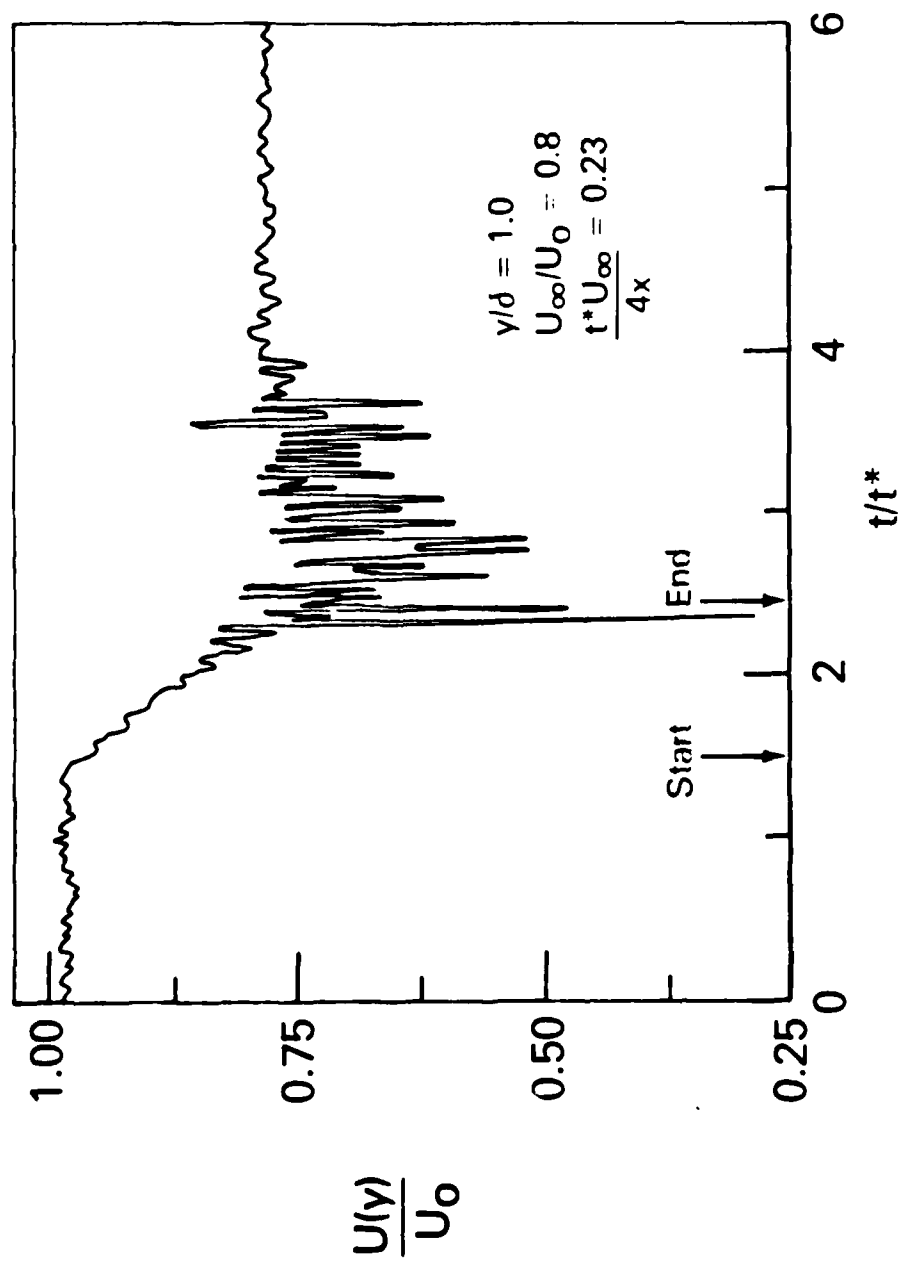
Figure 7.   Longitudinal Velocity Away From the Wall
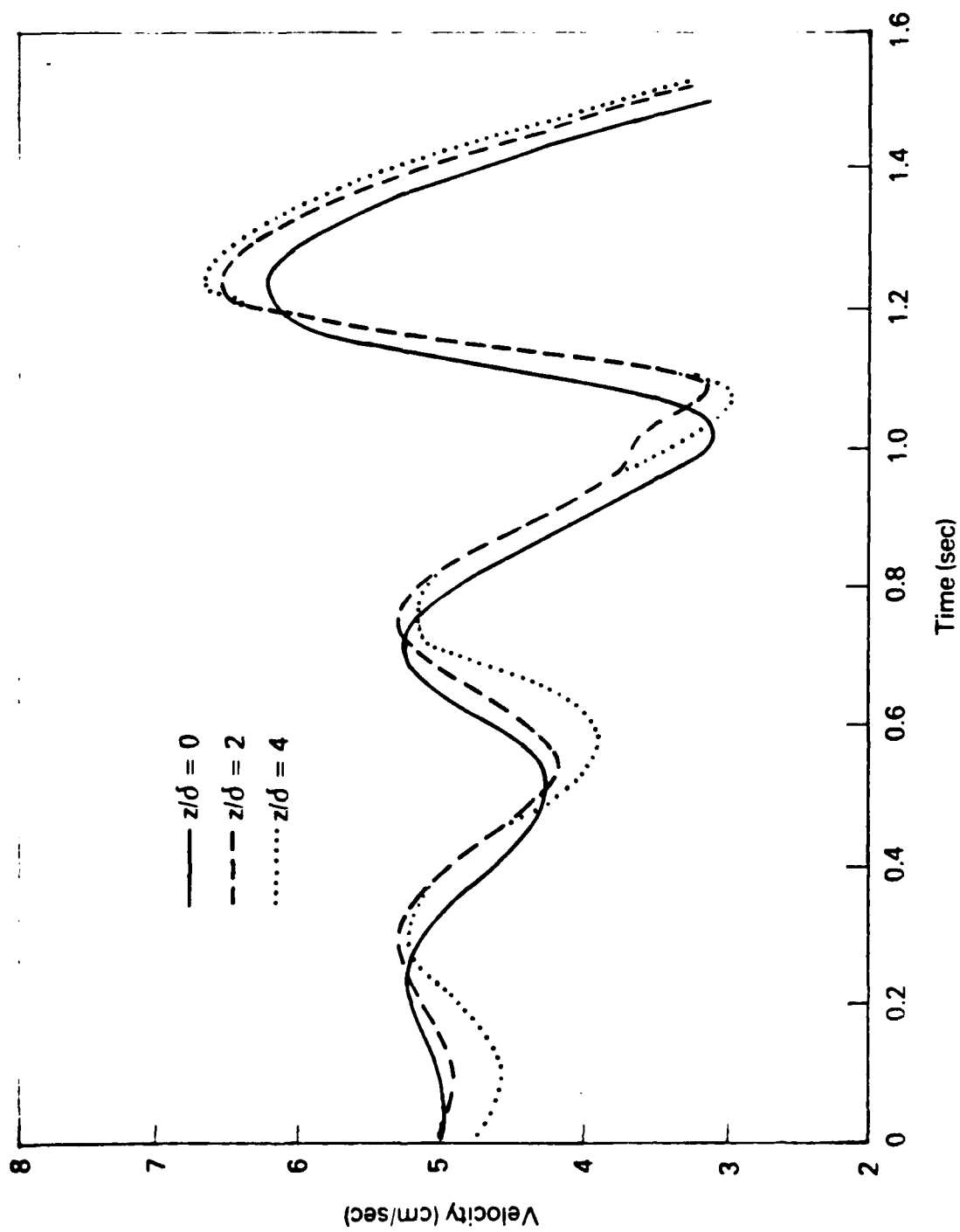
Figure 8. Spanwise Variations of the Instability Waves

Velocity (cm/sec)

Time (sec)

z/δ = 0
z/δ = 2
z/δ = 4
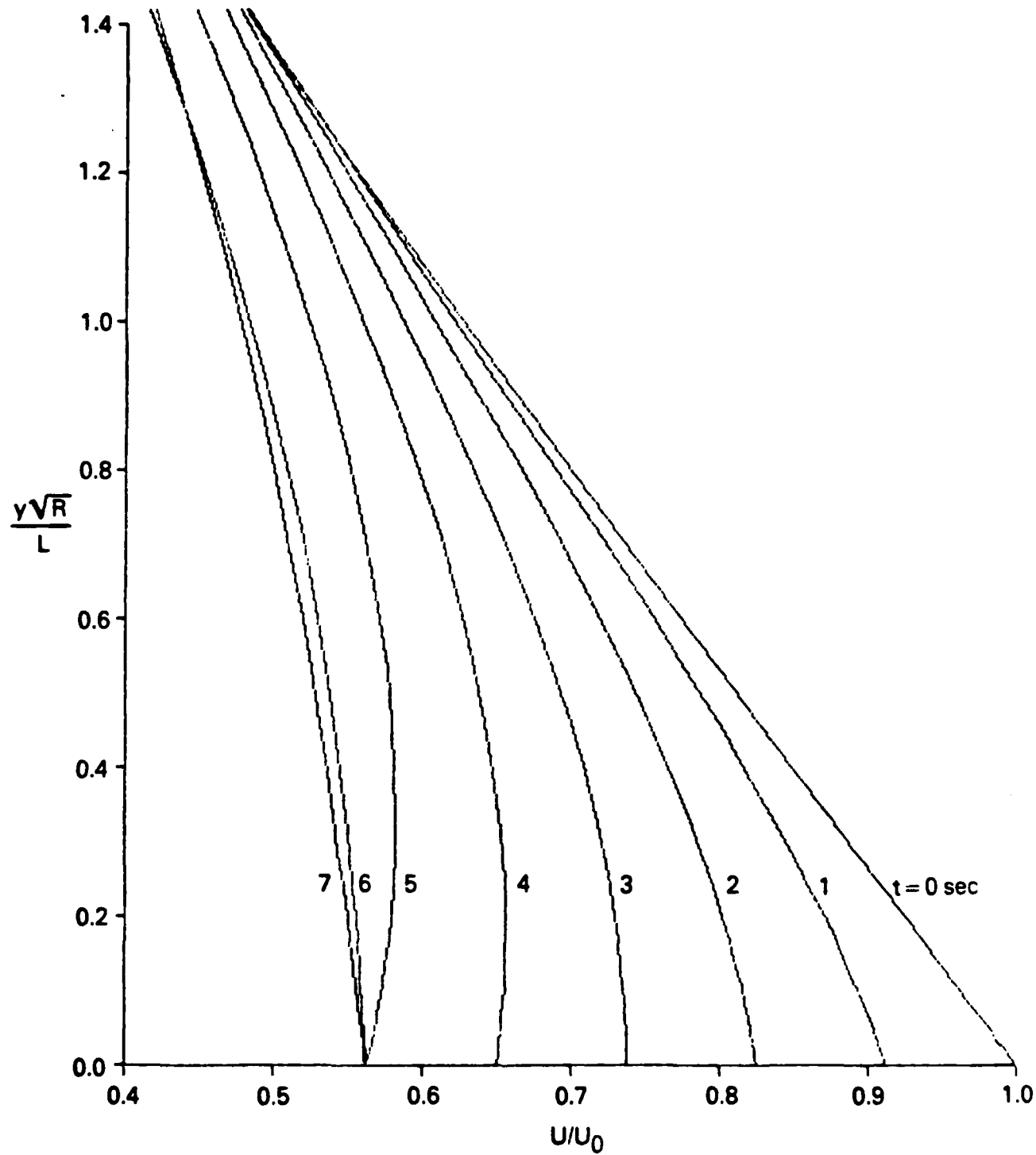
Figure 9. Typical Solution of the Unsteady Boundary Layer Equation
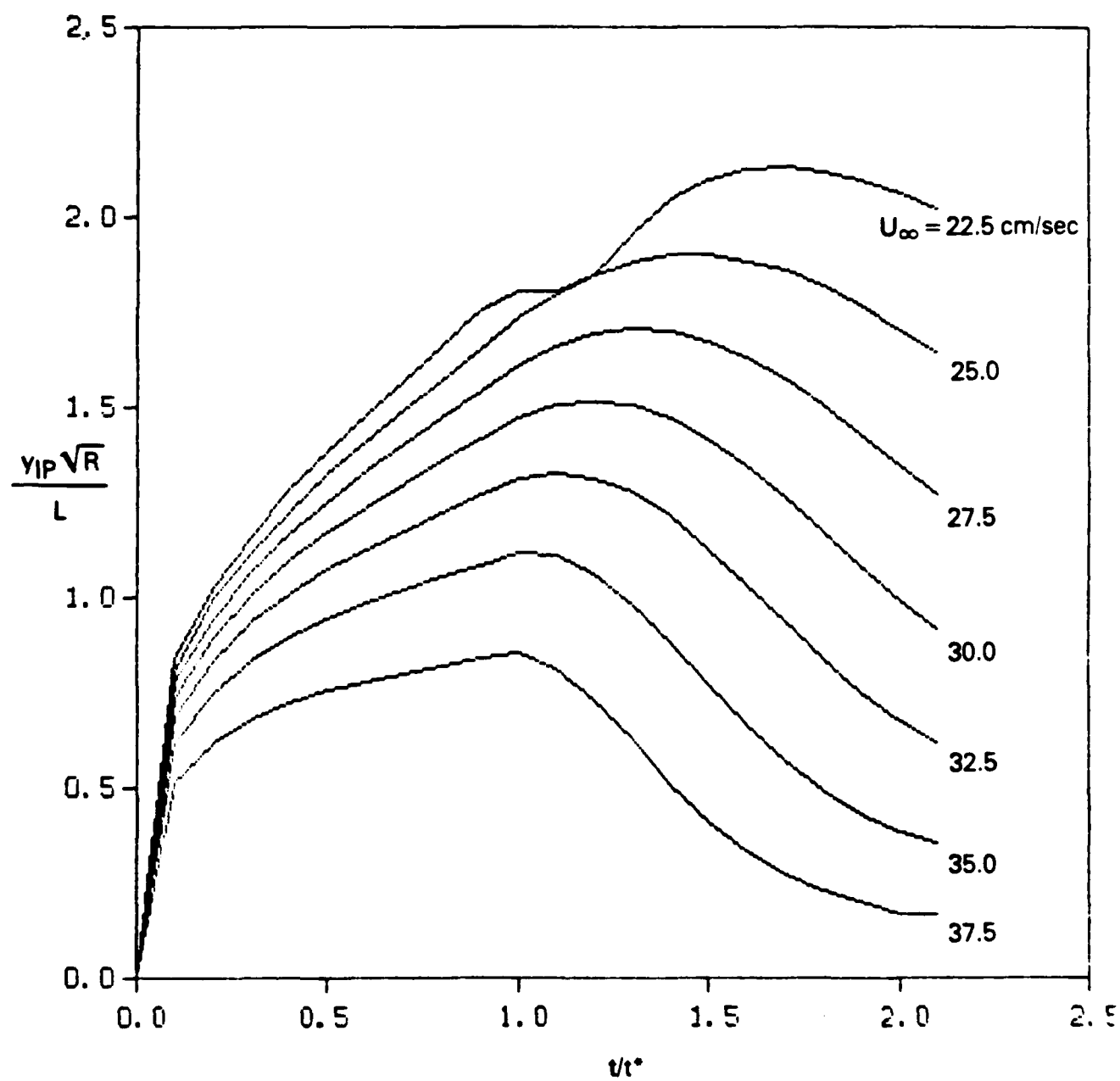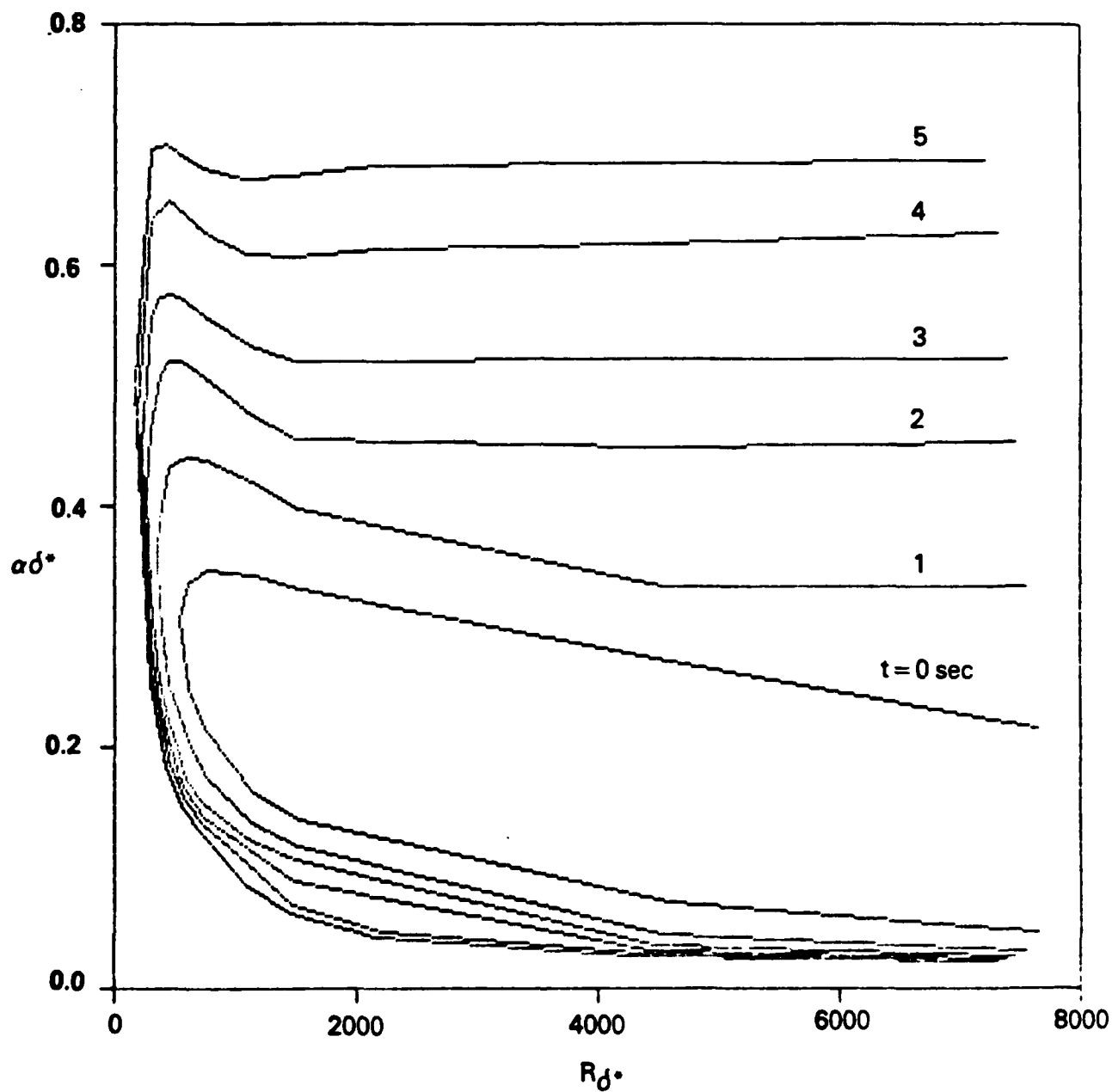
$U_0 = 40$ cm/sec, $U_\infty = 22.5$ cm/sec, $t^* = 5$ sec
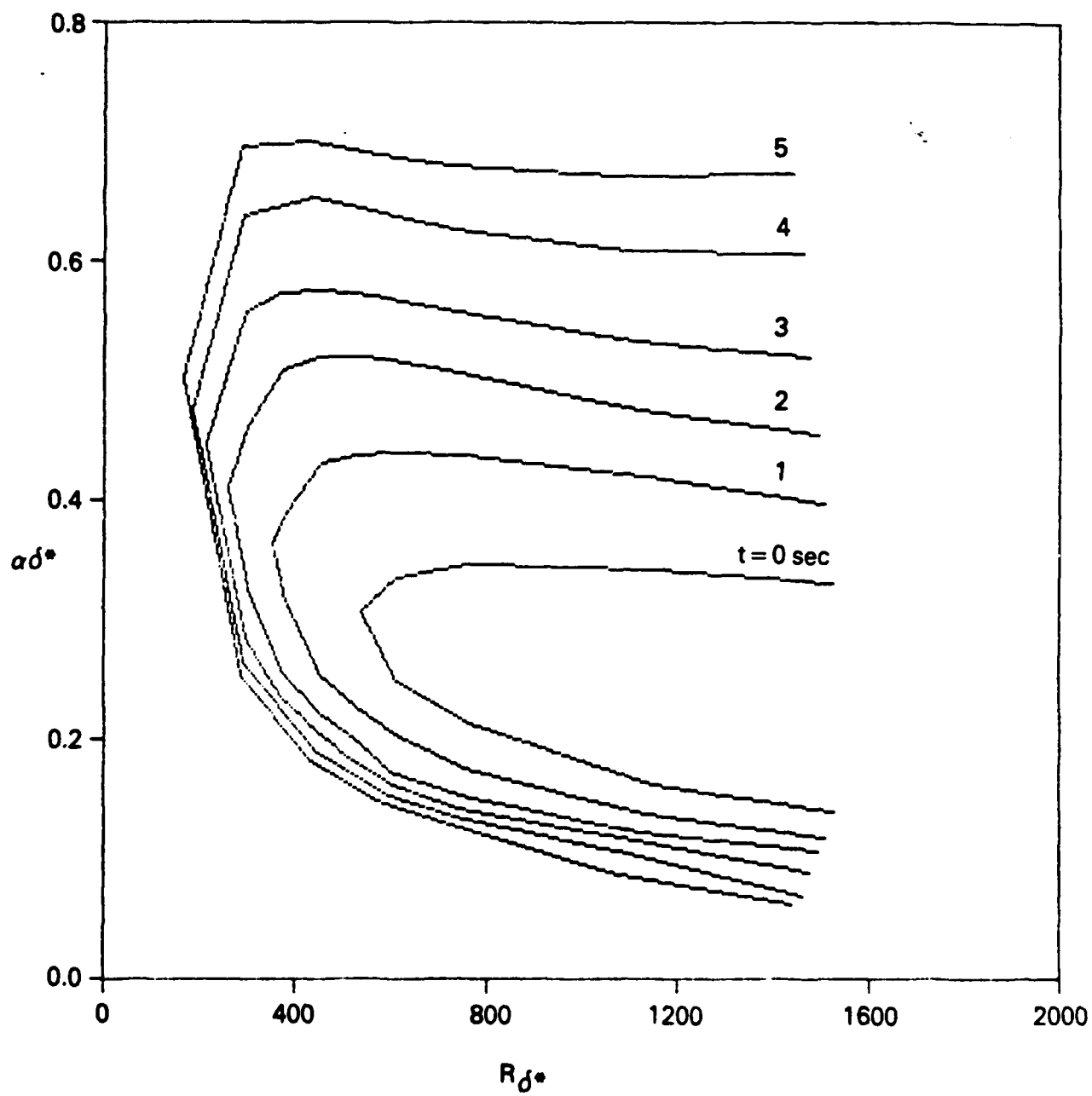
Figure 10. Migration of the Inflexion Point During Deceleration

$U_0 = 40$ cm/sec, $t^* = 5$ sec

Figure 11. Neutral Stability Curves During Deceleration

$U_0 = 40$ cm/sec, $U_\infty = 30$ cm/sec, $t^* = 5$ sec

Figure 11. Neutral Stability Curves During Deceleration (Cont.)

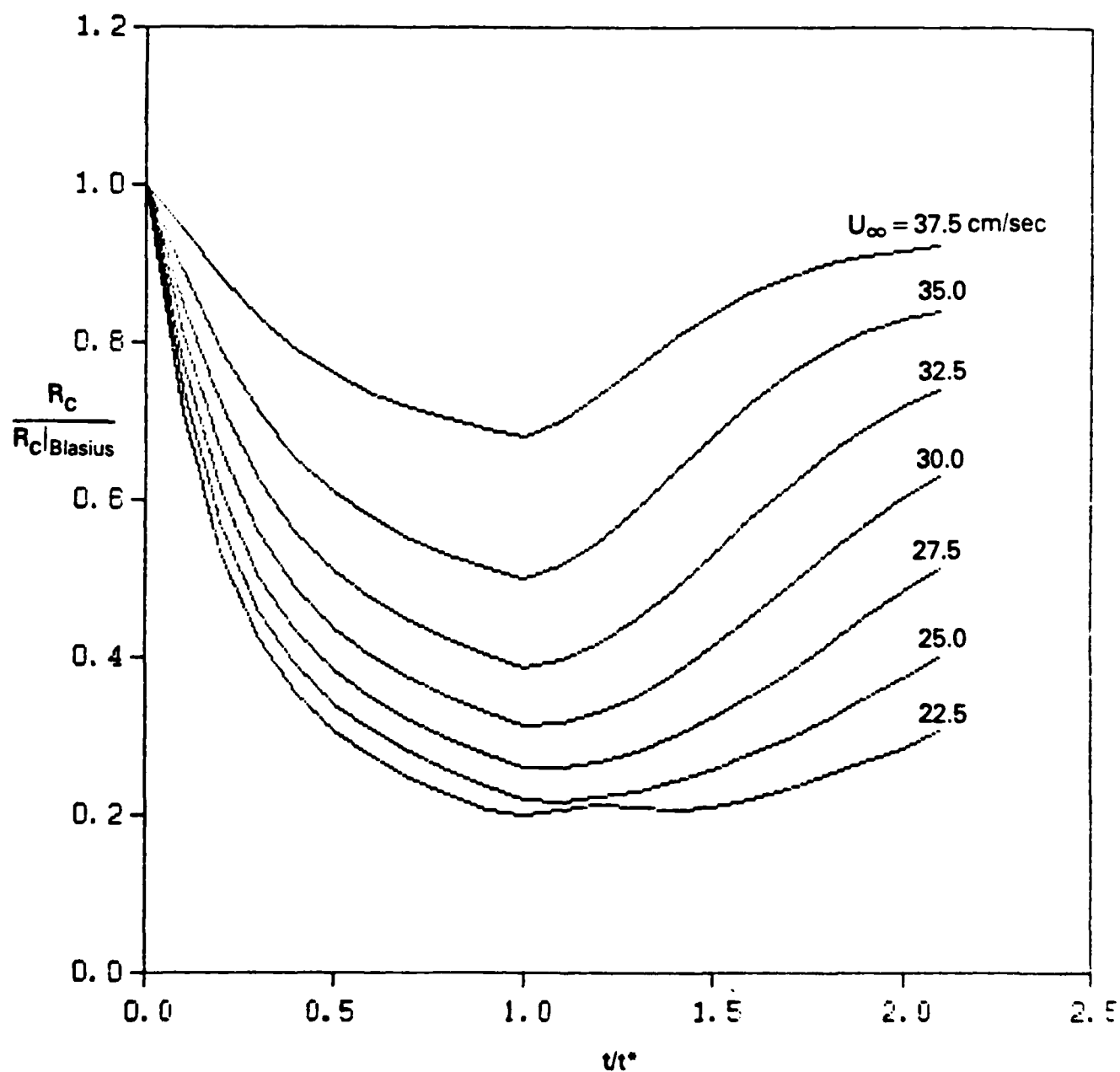$U_0 = 40$ cm/sec, $U_\infty = 30$ cm/sec, $t^* = 5$ sec

Figure 12. Plots of Critical Reynolds Number vs. Time
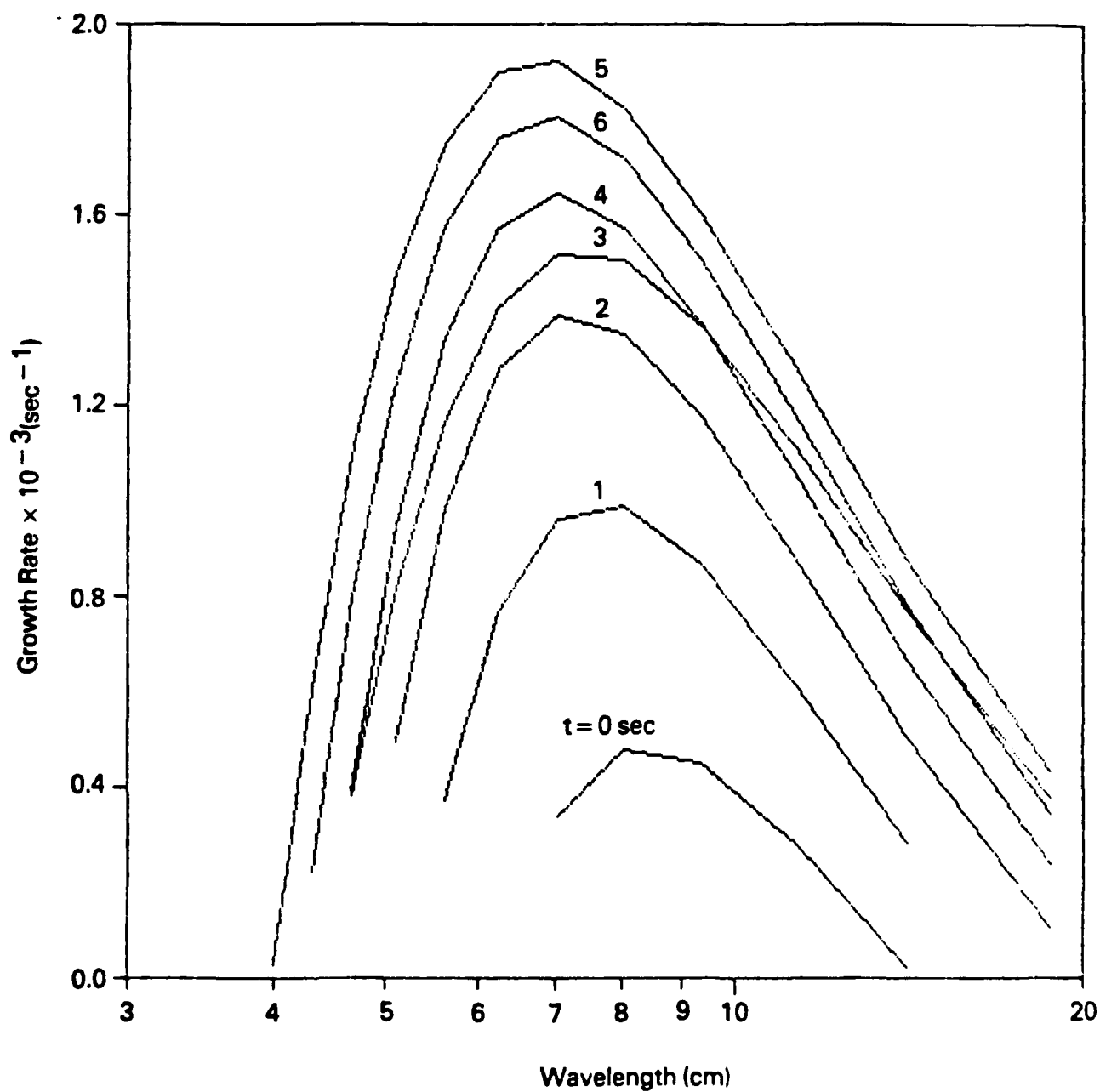
$U_0 = 40$ cm/sec, $t^* = 5$ sec

Figure 13. Plots of Growth Rate vs. Wavelength for the Unstable Modes
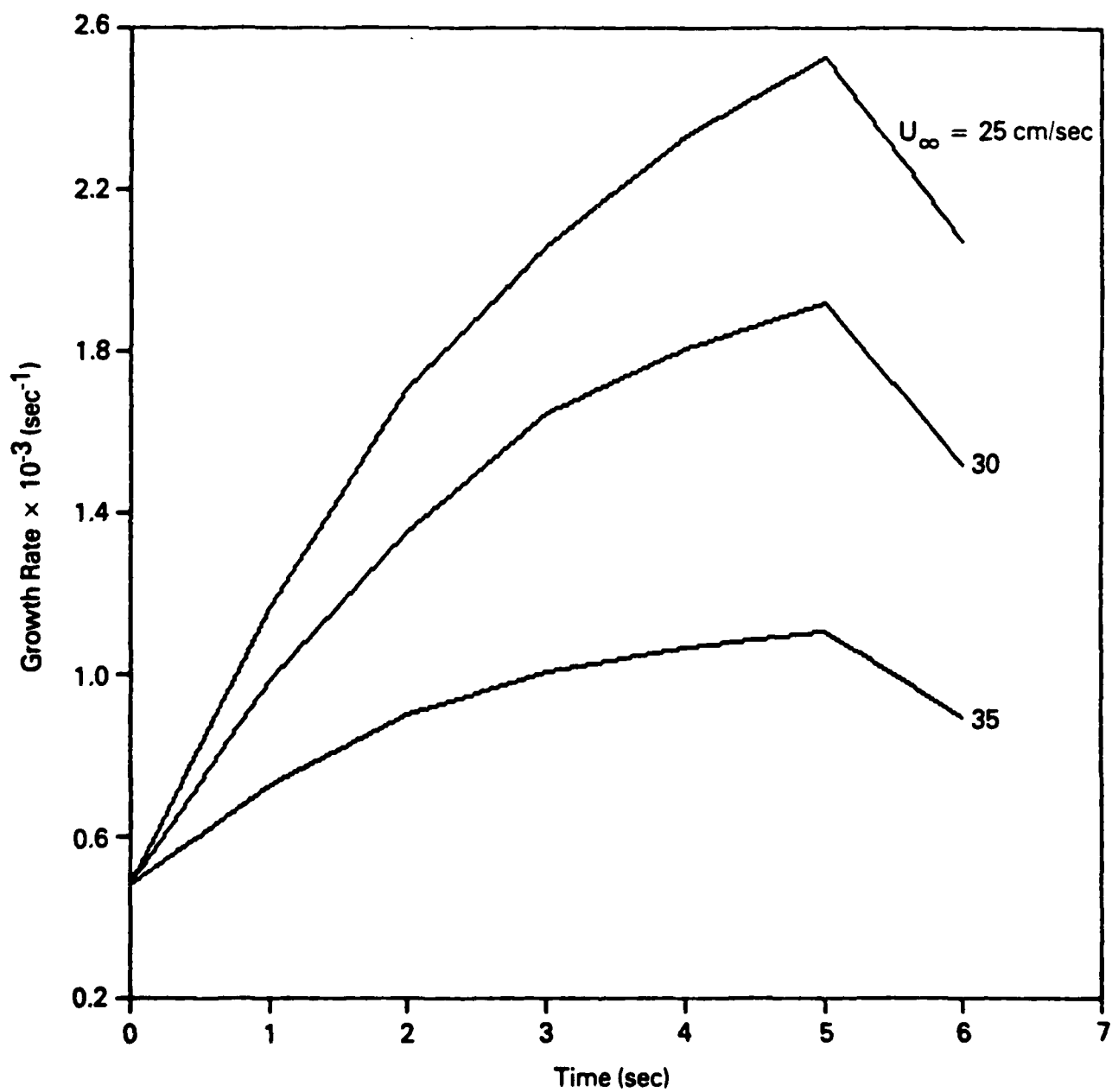
$U_0 = 40$ cm/sec, $U_\infty = 30$ cm/sec, $t^* = 5$ sec

Figure 14. Maximum Growth Rate During Deceleration
$U_o = 40$ cm/sec, $t^* = 5$ sec
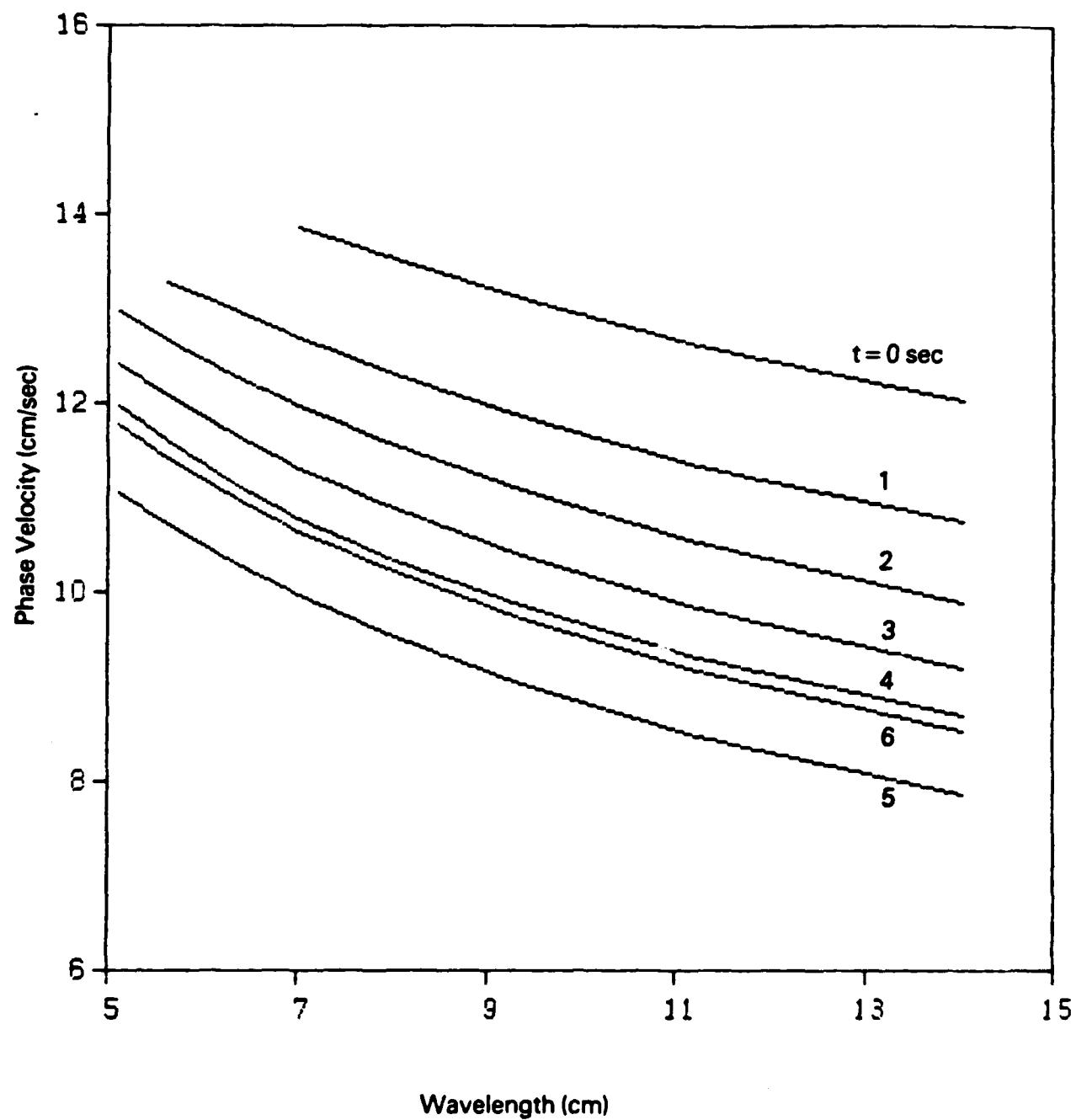
Figure 15. Plots of Phase Velocity vs. Wavelength for the Unstable Modes

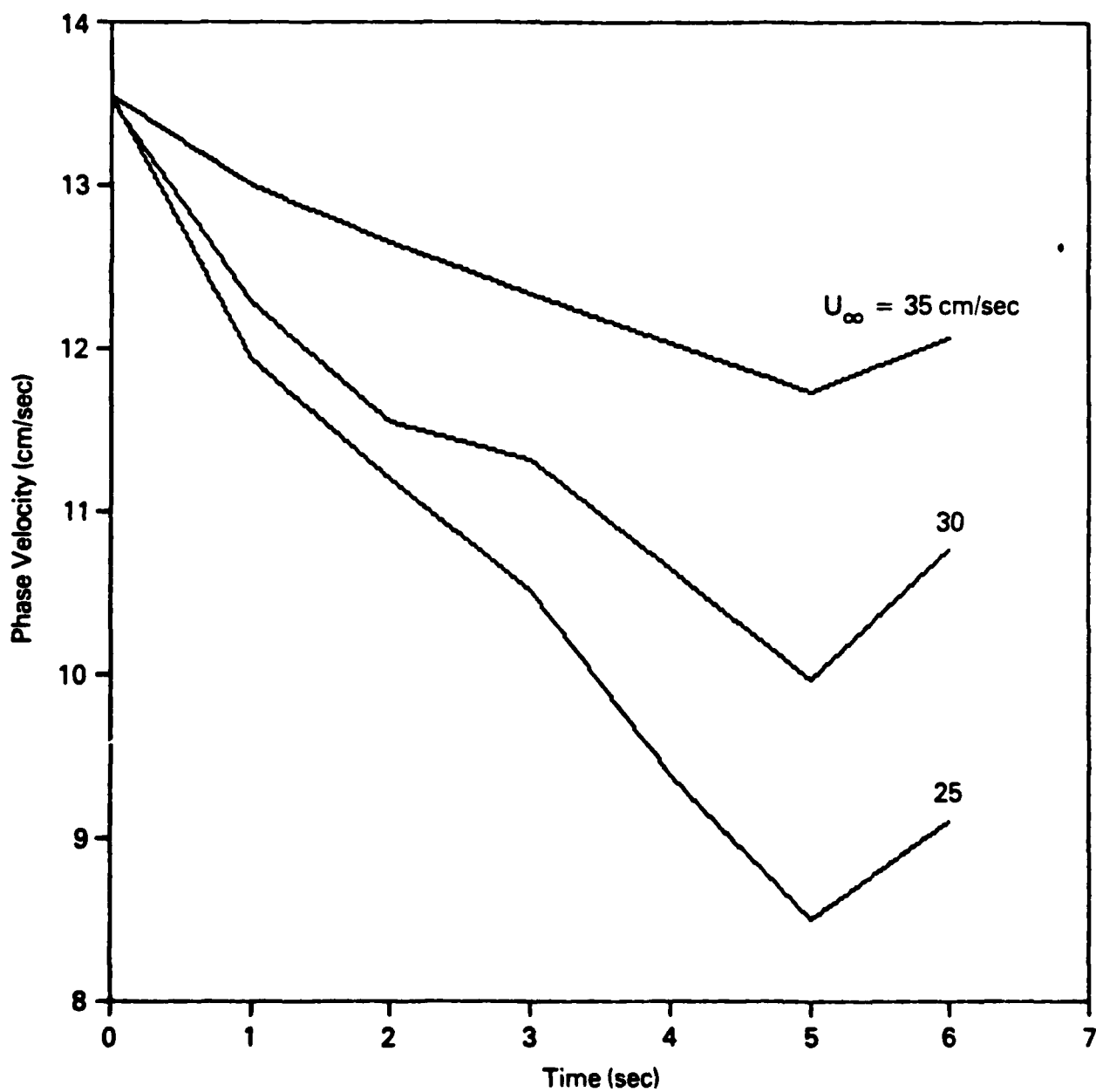$U_0 = 40$ cm/sec, $U_\infty = 30$ cm/sec, $t^\circ = 5$ sec

Figure 16. Phase Velocity of Most-Amplified Disturbance During Deceleration

$U_O = 40$ cm/sec, $t^* = 5$ sec

APPENDIX III

Preprint from the Proceedings of the Third
International Symposium on Flow Visualization

VISUALIZATION TECHNIQUES FOR STUDYING
TRANSITIONAL AND TURBULENT FLOWS*

M. Gad-el-Hak, R. F. Blackwelder** & J. J. Riley
Flow Research Company
Kent, WA 98032

A comparative analysis of different slot injection techniques were used
to visualize a transitional boundary layer. The methods included injecting
either conventional dye, a fluorescent dye excited by a sheet of laser light,
or reflecting micro-platelets which tend to align themselves with the instan-
taneous shear stress in the fluid. All three techniques were used to visualize
two different transitional flow fields; a turbulent wedge behind a single
roughness element and a turbulent spot developing in a laminar boundary layer.
Each method gives a different, unique and complementary view of the flow
structure.

1. Introduction

Flow visualization is the oldest method known for the study of fluid
mechanics. Historically, visualization methods have included fluid marker and
particle techniques. In the former method, a colored marker is injected into
the flow, with as little disturbance as possible, and the resulting streak
lines or sheets are observed to learn more about the flow field. In the second
technique, particles sufficiently small to follow the fluid motion are placed
in the flow field and their trajectories are followed to obtain information
about the fluid displacements and velocities. The major disadvantage of the
first method is that the observed marker illustrates the integrated history of
its motion and it is difficult to glean information about the present velocity
field. Consequently the observed results are often strong functions of the
point of injection. By tracking individual particles, on the other hand,

larger scale correlated motions associated with eddy structures are often overlooked because the particle responds equally well to the smaller scale uncorrelated motions.

During the past few decades many improvements have been made in flow visualization. In liquids, the use of photochromic dyes, fluorescent dyes, hydrogen bubbles, and related methods have been instrumental in increasing our understanding of low-speed fluid mechanics. Recently, a new visualization method of eddy structures in a transitional flow was reported by Carlson, Widnall and Peeters [1]. They filled a 0.6 cm x 80 cm x 410 cm channel flow with titanium-dioxide-coated mica platelets which were 10-20μ in diameter, 3-4μ thick, and had a specific gravity of 3. These disks were sufficiently small that they presumably align themselves with the instantaneous shear stress present in the fluid as long as the length scales of the eddy structures are greater than the dimensions of the platelets. Although the mica particles are larger, the technique is similar to the aluminum flakes used by Cantwell, Coles and Dimotakis [2].

In the channel flow study of Carlson et al. [1] a transitional turbulent region embedded within the laminar flow field was observed to grow as it moved downstream similar to the turbulent spot in a transitional laminar boundary layer. Waves were observed to emanate from the turbulent region into the surrounding laminar flow. The waves were oblique with respect to the mean flow and were the predominate structure observed in the photographs. Since they had not been observed before using more conventional visualization techniques, it was conjectured that similar wave patterns may be present in a transitional boundary layer flow. Thus the present comparative study in boundary layers was undertaken to determine if this new technique might divulge some new information on turbulent regions in a transitional boundary layer.

2. Experimental Apparatus

The visualization tests were conducted in a towing tank that is 1.2 m wide, 0.9 m deep and 18 m long as described by Gad-el-Hak, Blackwelder and Riley [3]. The flat plate plexiglas test model was 210 cm long and 106 cm wide and had a trailing edge flap to adjust the stagnation point on the working side of the elliptical leading edge. The streamwise coordinate, x, is taken from the leading edge, y is perpendicular to the plate and z is the spanwise coordinate. The plate was aerodynamically smooth so that natural transition only occurred at $Re_x > 10^6$. Turbulent wedges were formed behind 1.0 cm diameter, 0.6 cm high cylindrical roughness elements placed at x = 120 and 128 cm.

Turbulent spots were initiated by small momentary jets of fluid emanating from a 0.5 mm hole 46 cm downstream of the leading edge. The plate was towed at 25 cm/sec in the experiments reported here.

For the mica platelets experiments, a water suspension of the platelets was made at a concentration of 2% by weight. This suspension and the dyes were injected through two different slots located at x = 75 cm and x = 123 cm. Each slot was inclined 45° with respect to the downstream direction and had a slot width of 0.4 mm. The upstream slot spanned 50 cm and the downstream slot was 15 cm wide.

In the fluorescent dye experiments, a dye (trade name Fluorescein) was excited by a 5 watt argon laser (Spectra Physics, Model 164). A sheet of light 1 mm thick in the x-z plane was produced by reflecting the laser beam from a small mirror which oscillated at 500 Hz. Flood light illumination was used for the conventional food coloring dye (Red dye No. 40). Six 600 watt flood lights were projected onto the plate from an acute angle of 45° with respect to the y axis. For the platelets, four 600 watt lamps were aligned parallel to the x axis on each side of the tank at y = 0.

Photographic records of the flow fields were obtained using 35 mm cameras and also 16 mm cine films. Both cameras were located perpendicular to the plate over the desired streamwise location.

3. Turbulent Wedge Results

Figures 1, 2 and 3 show the flow field behind roughness elements for the conventional dye, the platelet suspension and the Fluorescein dye respectively. In all three cases, one roughness element is located 3 cm upstream and one 5 cm downstream of the dye slot. The roughness element introduces a horseshoe vortex into the flow field with its legs downstream of the element. First, consider the element positioned after the injection of the marked fluid. The horseshoe vortex removes the dye from the wall directly upstream and to the sides of the element. This fluid is displaced upward as the vortex continues to wrap the marked fluid around its legs, leading to a different visualization in all three cases. In the conventional dye method, Figure 1, an integrated view across the entire boundary layer is seen. The marked fluid gives the appearance that the wake is narrower 3-6 diameters downstream than is indicated by the other figures. Further downstream, filaments of dye are seen crossing the wake at oblique angles. In Figure 2, the additional platelets in the edges of the wake 3-6 diameters downstream are aligned by the stress imposed by the legs of the vortex. Being aligned perpendicular to the light

source provides greater reflection and hence a sharper contrast in that region. In Figure 3, the sheet of laser light is 5 mm above the wall. Consequently no visual results are obtained until the flow field elevates the Fluorescein to that location. In addition, the relaxation time of the stimulated dye is much shorter than the time scales in the flow, so only dye within the laser sheet is seen. The turbulent structure observed in Figure 3 must be associated with the filaments of dye seen in the integrated view of Figure 1.

The roughness elements placed upstream of the injection slot create a different image of the wake. In all three figures, this configuration shows that the wake is much more turbulent than it appears behind the downstream element even though the wake structure must be similar in both cases since their Reynolds numbers are comparable. This results from the marker being injected into the flow after it had become turbulent in contrast to the previous case in which the marker was injected into a laminar flow that subsequently became turbulent. In all three figures, the horseshoe vortex around the downstream element removed the marked particles from the wake region prior to transition thus creating a wake devoid of marked particles. The contrast in each figure illustrates that the present location of the marker is a strong function of its past history which can make it difficult to obtain quantitative data from such photographs.

4. Turbulent Spot Results

When initiated from a point source in an unstable laminar boundary layer, it is well documented that a turbulent spot maintains an arrowhead shape as it grows downstream. Examples of this classical phenomenon are shown in Figures 4, 5 and 6 for the conventional dye, the platelet suspension and the Fluorescein dye respectively. The classical arrowhead-shaped patch of turbulence is readily apparent in all three figures; however each technique displays different features. In Figure 4, the dye provides a spatially integrated view of the turbulent spot, without any details of its internal structure. The tips of the spot, i.e. the spanwise extremities, are relatively darker because they are continually engulfing new marked fluid as the spot moves downstream. In the triangular-shaped region behind the spot where the velocity profiles are stable [4], thin streamwise filaments of dye are observable. These are felt to be remnants of streamwise vortices associated with the spot.

The eddy structure within the spot appears more vividly when visualized with the platelet solution as seen in Figure 5. The approximately instantaneous response of the mica platelets is particularly more evident around the leading

edges of the spot, where much more details of the breakdown of laminar fluid
into turbulence are observed. In the calmed region, the elongated streamwise
streaks are present at least 1-1/2 spot lengths upstream as in Figure 4. Since
the streaks disappear approximately one second after the spot passage, their
disappearance may be due to the relaxation time of the platelets rather than
the disappearance of a strong stress associated with streamwise vortices. The
regions near the tips appear to contain more randomness suggesting a greater
mixing. Similar results were also found by Carlson et al. [1] in turbulent
regions developing in plane Poiseuille flow.

A cross sectional slice of the spot visualized by a sheet of light roughly
5 mm above the wall is seen in Figure 6. As in Figure 3, no manifestation of
the spot is evident until the dye has been elevated into the light sheet.
When the light sheet was lower, as in Gad-el-Hak et al. [3], evidence of the
trailing streaks was quite evident. Since they are not as prominent in
Figure 6, the streaks must only occur very near the wall. Near the edges of
the spot the dye lines are sharp, indicative of the initial breakdown into
chaotic motion. Toward the middle of the spot, the dye becomes more diffused
because the turbulence there is older and more mixing has occurred.

The platelet solution was used to obtain the magnified view of the nose
of the spot seen in Figure 7. A higher flow rate through the injection slot
was used than for Figure 5; consequently a different impression of the
turbulent spot is obtained. Disturbances in the laminar flow are seen before
the breakdown into turbulence becomes apparent. With suspensions having higher
concentrations of platelets, these disturbances are seen further upstream as
found by Cantwell et al. [2]. Inside the spot, greater evidence of the turbu-
lence is seen in Figure 7 than in Figure 5.

Figure 8 shows a magnified section of the spot's nose at an elevation of
5 mm using Fluorescein dye. Greater detail of the turbulent eddies can be seen
in this slice through the spot compared to the integrated view in Figure 7.
Since the dye has not been elevated into the sheet of laser light, the precur-
sive disturbances ahead of the spot are not seen here.

5. Conclusions

Comparing results from the three marker techniques illustrate that each
responds differently to the same flow field. The conventional dye is strictly
passive and always provides a spatially integrated view of the observed
structure. Thus, details of the internal structure of the flow field are
difficult to obtain. The Fluorescein dye disperses in the same manner as the

conventional dye, but is only observed when excited by light of a given wave-
length. By using sheets of such light, cross-sectional views of the flow can
be obtained, yielding greater detail of the eddy structures. The platelet
suspension is dispersed as are the two dyes. But the platelets align them-
selves with the shear stress imposed upon them by the flow, thus giving a more
instantaneous view of the stress within the flow field. Since they reflect
the imposed illumination, the platelet results also depend, to some extent, on
the direction of the illumination.

The visual images obtained by all three techniques are sensitive to the
flow rate at the injection slot. The only known systematic study of this para-
meter has been by Oldaker and Tiederman [5] during a study of low-speed streaks
in a turbulent flow. Comparison of Figures 5 and 7 indicate that this parameter
is quite important in interpreting visual results and understanding the eddy
structure in the near wall region. For example, with the low injection rate in
Figure 5, streamwise streaks are observed under the nose whereas with the higher
injection rate in Figure 7, eddy structures similar to Falco' pockets [6] are
seen.

Lastly, no wave structure comparable to that reported by Carlson et al.
[1] was found surrounding a turbulent spot in a laminar boundary layer suggest-
ing that they may be only manifested in the transitional channel flows and not
in boundary layers. However, this result can not be regarded as conclusive
because the waves may be on a higher elevation above the wall than the slot
injected particles and thus would not be visualized. The trailing waves of
Wygnanski, Haritonidis and Kaplan [7] were also not observed for possibly the
same reason.

References

1. Carlson, D. R., Widnall, S. E. and Peeters, M. F., J. Fluid Mech. 121,
    487, 1982.

2. Cantwell, B., Coles, D. and Dimotakis, P., J. Fluid Mech. 87, 641, 1978.

3. Gad-el-Hak, M., Blackwelder, R. F. and Riley, J. J., J. Fluid Mech. 110,
    73, 1981.

4. Schubauer, G. B. and Klebanoff, P. S., NACA Report No. 1289, 1956.

5. Oldaker, D. K. and Tiedermann, W. G., Physics of Fluids 20, S133, 1977.

6. Falco, R. E., Coherent Structure of Turbulent Boundary Layers, Ed.
    C. R. Smith and D. E. Abbott, Lehigh Univ., 448, 1978.

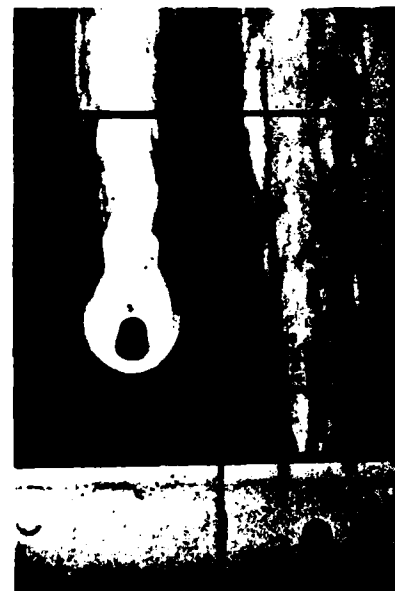7. Wygnanski, I., Haritonidis, J. H. and Kaplan, R. E., J. Fluid Mech. 92,
    505, 1979.

Figure 1. Turbulent Wedges behind Two Roughness Elements Placed Upstream and Downstream of a Conventional Dye Slot

FLOW

Figure 2. Similar to Figure 1 with the Marker being Micro-Platelets

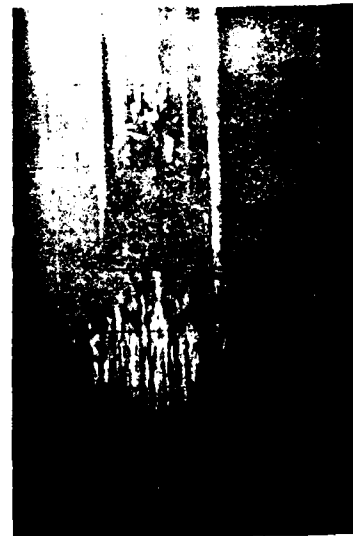Figure 3. Similar to Figure 1 but Using Fluorescent Dye Excited by a Sheet of Laser

FLOW

Figure 4. A Turbulent Spot Visualized Using Conventional Food Color Dye

Figure 5. Similar to Figure 4 with a Suspension of Micro-Platelets Used for Visualization

Figure 6. Similar to Figure 4 Except Fluorescent Dye is Used for Visualization

Figure 7. Magnified View of the Spot's Nose Using the Platelet Suspension

Figure 8. Similar to Figure 7 Visualized with Fluorescent Dye and a Sheet of Laser

FLOW

FLOW